Inorganica Chimica Acta 363 (2010) 1157–1172

Contents lists available at ScienceDirect

Inorganica Chimica Acta

journal homepage: www.elsevier.com/locate/ica

Synthesis and structural investigations of Ni(II)- and Pd(II)-coordinated α-diimines with chlorinated backbones

Sofia I. Pascu [a,*], Gabor Balazs [b], Jennifer C. Green [b,*], Malcolm L.H. Green [b,*], Ino C. Vei [b], John E. Warren [a,c], Caroline Windsor [b]

[a] *Department of Chemistry, University of Bath, Claverton Down, Bath BA2 7AY, UK*
[b] *Department of Chemistry, Inorganic Chemistry Laboratory, University of Oxford, South Parks Road, Oxford OX1 3QR, UK*
[c] *Synchrotron Radiation Source, Daresbury Laboratory, Warrington WA4 4AD, UK*

ARTICLE INFO

Article history:
Received 1 June 2009
Received in revised form 30 October 2009
Accepted 8 November 2009
Available online 14 November 2009

This paper is dedicated to Professor Jon Dilworth on the occasion of his 65th birthday.

Keywords:
Pd(II) complexes
Halide-substituted α-diimines
Ethylene polymerisation catalysts
Heterobimetallic early–late transition metal complexes
Density functional theory

ABSTRACT

Novel square planar Pd(II) α-diimines $[PdX_2\{ArN{=}C(Cl)\}_2]$, where Ar = C_6H_5, $(2,6\text{-}Me_2C_6H_3)$, $(2,6\text{-}{}^iPr_2C_6H_3)$ and X = Cl or Br, and the octahedral Ni(II) complex $[NiBr_2\{(C_6H_5)N{=}C(Cl)\}_2(THF)_2]$ have been prepared and characterised by spectroscopic methods. For two of the Pd(II) complexes and the Ni(II) complex the crystal structures were determined by X-ray crystallography. A further insight into the geometry and electronic structure of $[PdBr_2\{(2,6\text{-}Me_2C_6H_3)N{=}C(Cl)\}_2]$ was gained using density functional theoretical calculations (DFT). This compound resembles structurally and electronically typical olefin polymerisation pre-catalysts supported by α-diimines incorporating methyl- and 1,8-naphtalenyl substituents at the ligand backbone. The chlorine-substituted backbone of the free ligand $[2,6\text{-}Me_2C_6H_3N{=}C(Cl)]_2$ can be employed in further alkylation reactions to generate new multifunctional ligand prototypes with potential uses as *ansa*-metallocene/diimines building blocks for catalytic applications of heterobimetallic complexes.

1. Introduction

The interest in the chemistry of 1,4-disubstituted-1,4-diaza-1,3-butadienes (R-DAB) and in their metal complexes was boosted by the discovery by Brookhart and co-workers of highly active Ni(II) and Pd(II) α-olefin polymerisation catalysts containing bulky diimine ligands of this family [1–6]. Ligands with R^2, R^3 = H, alkyl, aryl, 1,8-naphthalenyl (Fig. 1) have been explored in this context, showing versatile coordination behaviour and a wide variety of reactivity patterns, which was assigned to their interesting electronic properties.

Various synthetic routes for R-DAB ligands enabled the preparation of an array of ligands with different R^1–R^3 substituents, which allowed both the steric and electronic properties to be varied. These ligands were shown to have a versatile chemistry, acting as N σ-donors or as η^2-C=N π-donors. The torsional isomers of R-DAB type ligands, *s-cis* and *s-trans*, adopt conformations shown in Fig. 1. The steric properties of R^1, R^2 and R^3 substituents influence the stability of the N=C–C=N conformation and therefore the metal coordination abilities and the reactivity of the resulting complexes. Many examples of α-diimines with a rigid backbone, where rotation around the C–C backbone is restricted to give the *s-cis* orientation, have also been reported and their metal complexes have been tested as olefin polymerisation and other organic reaction catalysis [2–4,7].

Despite a large number of reports concerning the organic chemistry of oxazolyl chlorides, which are known since 1907 [8], there are only a handful of reports on the ability of (N-coordinated) transition metals to mediate their reactivity in organic transformations involving the C(Cl)–C(Cl) backbone [9–15]. The chemistry of halide-substituted diimines (e.g. R^2, R^3 = Cl) is virtually unexplored in the context of their metal coordination chemistry. Their catalytic activity or use as potential building blocks towards the synthesis of more complex potentially heterobimetallic systems with catalytic applications towards organic reactions has not been explored. The reactivity of metal-coordinated oxazolyl chlorides has not been investigated thus far. To the best of our knowledge, there are only very few structural investigations concerning the metal complexes of this class of chlorine-substituted diimines, such as, for example, the complexes $[NiBr_2(\{(p\text{-}Tol)(C_6H_4)N{=}C(Cl)\}_2)(THF)_2]$, $[NiBr_2(\{(2\text{-}(C_6F_5)C_6H_4)N{=}C(Cl)\}_2)(OH_2)_2]$, and $[CoBr_2(\{(2\text{-}(C_6F_5)C_6H_4)N{=}C(Cl)\}_2)]$ [13,14].

---

* Corresponding authors. Tel.: +44 1225386627 (S.I. Pascu).
E-mail address: s.pascu@bath.ac.uk (S.I. Pascu).

0020-1693/$ - see front matter © 2009 Elsevier B.V. All rights reserved.
doi:10.1016/j.ica.2009.11.009

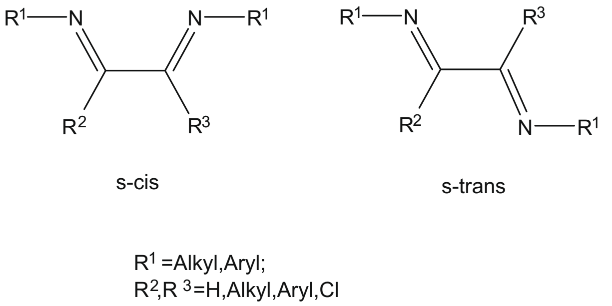

Fig. 1. Geometric isomers of typical α-diimines.

Here we report the synthesis of novel Group 10 metal complexes in the family of α-diimines ($R^2 = R^3 = Cl$) and compare their reactivity, catalytic behaviour towards olefin polymerisation and electronic properties and with those of (typical Brookhart-type) α-diimine pre-catalysts with R^2, R^3 = Me or 1,8-naphthalenyl with related geometries. We are also interested in designing ligands that can render active one or both of the metal centres in a potentially heterobimetallic catalyst for organic reactions. When the two metal centres are held in close proximity by the ligand, they can co-operate in the transition state of the reaction, thus having the potential for catalysing reactions more efficiently, or with different chemo-, regio- or stereo-selectivity than found for mononuclear species [16–19] and there has been an increase in the study of the reactivities of complexes containing two different metal centres [18,20–22]. It is well established that both *ansa*-metallocenes and α-diimine complexes are good catalysts for ethylene polymerisation the first giving linear and the latter giving branched polyethylene [1–4,23,24]. Combining two types of catalytic centres: early transition metal systems (such as metallocenes) and late transition metal centres (i.e. supported by chelating diimines) [25] could result in polymeric materials with new and useful characteristics thus far unexplored. To date, promising ligands suitable to tackle this problem have not been discovered. Only a limited number of early–late heterobimetallic systems have been isolated and ligand frameworks suitable to act as precursors for 'two-in-one' *ansa*-metallocene/diimine systems are currently unavailable. The halide-substituted diimines (also called oxazolyl chlorides or bis-imodoylchlorides) are already of interest as building blocks to generate such ligands, since there are a number of reports on their further organic chemistry derivatisation via substitution reactions at their C(Cl)–C(Cl) backbone [9–15].

We report here an efficient route to a new class of organic ligand precursors combining both α-diimines and fluorenyl functional groups in the same molecule. This system could potentially lead to new heterobimetallic complexes, with properties thus far unexplored, incorporating an *ansa*-metallocene site (known to effectively bind early transition metals) and an α-diimine (known to coordinate efficiently to late transition metal complexes).

2. Results and discussions

2.1. Synthesis and spectroscopic characterisation

The α-diimine ligands PhN=C(Cl)—C(Cl)=NPh (**1**) ($2,6\text{-}Me_2C_6H_3$)N=C(Cl)C(Cl)=N($2,6\text{-}Me_2C_6H_3$) (**2**) and ($2,6\text{-}{}^iPr_2C_6H_3$)N=C(Cl)-C(Cl)=N($2,6\text{-}{}^iPr_2C_6H_3$) (**3**) were prepared following modifications of the literature procedures [13,26]. The crucial step in the synthesis of these bis-imodoylchlorides is the isolation of the relevant oxalamides RN(H)C(=O)–C(=O)(H)NR. These were prepared by reaction of the corresponding amine R–NH_2 with ClC(=O)–C(=O)Cl in Et_2O. In each case, the resulting white precipitate was isolated by filtration and, after washing with Et_2O and light petroleum ether (b.p. 40–60 °C), the compounds RN(H)C(=O)–C(=O)(H)NR, where R = Ph, Me, ${}^iPr$, were obtained in good yield. After treatment with PCl_5 and work-up, the desired ligands **1–3** were isolated as bright-yellow microcrystalline powders in yields comparable with the reported methods (60–65%) [13,26].

The metal complexes **4–8** were synthesised according to Scheme 1. When a suspension of [$NiBr_2$(DME)] in THF was added to PhN=C(Cl)–C(Cl)=NPh, a dark orange reaction mixture was obtained. After filtration, all volatiles were removed under reduced pressure and the solid was washed with pentane. The crude product was recrystallised from THF/pentane to afford [$NiBr_2${PhN=C(Cl)}$_2$(THF)$_2$] (**4**) and this was supported by X-ray crystallography.[1]

A solution of [PhN=C(Cl)–C(Cl)=NPh] (**1**) in CH_2Cl_2 was added to a solution of [$PdCl_2(PhCN)_2$] in CH_2Cl_2 at room temperature. The resulting orange precipitate was isolated, washed with pentane and recrystallised from CH_2Cl_2/pentane. The complex [$PdCl_2${PhN=C(Cl)}$_2$] **5** was isolated as an orange crystalline solid in 40% yield. Treatment of [$PdCl_2(PhCN)_2$] with [($2,6\text{-}Me_2C_6H_3$)N=C(Cl)–C(Cl)=N($2,6\text{-}Me_2C_6H_3$)] (**2**) in CH_2Cl_2 gave an orange solution. After 12 hours of stirring under N_2, the volatiles were removed under reduced pressure and the resulting solid was washed with pentane. After recrystallisation of this residue from CH_2Cl_2/pentane the complex [$PdCl_2${($2,6\text{-}Me_2C_6H_3$)N=C(Cl)}$_2$] (**6**) was obtained as an orange solid in moderate yield (40%).

A THF solution of [ArN=C(Cl)]$_2$ (where Ar = $2,6\text{-}Me_2C_6H_3$ (**2**) or $2,6\text{-}{}^iPr_2C_6H_3$ (**3**)) was added to a slurry of [$PdBr_2$] in THF at −78 °C. Reactions were carried out using 1:1 ratios of the reactants, to give [$PdBr_2${($2,6\text{-}Me_2C_6H_3$)N=C(Cl)}$_2$] (**7**) and [$PdBr_2${($2,6\text{-}{}^iPr_2C_6H_3$)N=C(Cl)}$_2$] (**8**) respectively, both as orange solids. A significantly lower yield was obtained in the case of the **8** with respect to 7 (ca. 3% compared with 31%). This is presumably due to the steric hindrance of the ${}^iPr$ substituents in [($2,6\text{-}{}^iPr_2C_6H_3$)N=C(Cl)–C(Cl)=N($2,6\text{-}{}^iPr_2C_6H_3$)] (**8**).

The compounds [PdX_2{(Ar)N=C(Cl)}$_2$)], where X = Cl, Ar = C_6H_5 (**5**) and $2,6\text{-}Me_2C_6H_3$ (**6**), and X = Br, Ar = $2,6\text{-}Me_2C_6H_3$ (**7**) and $2,6\text{-}{}^iPr_2C_6H_3$ (**8**) were all characterised by elemental analysis, IR and NMR spectroscopies. The ^1H NMR spectrum of **5** in d_6-DMSO consists of three multiplets at δ 7.54, 7.35 and 7.15 ppm, which are assigned to the *m*-, *p*- and *o*-protons of the phenyl ring respectively. The $^{13}C\{^1H\}$ NMR spectrum in the same solvent shows four peaks at δ 137.41, 128.64, 124.51 and 120.24 ppm. The use of ^1H–^{13}C HMBC and ^1H–^{13}C HMQC experiments revealed that these signals correspond to the *ipso*-, *p*-, *o*- and *m*-carbons of the phenyl rings, respectively. Peaks corresponding to the quaternary carbon atoms of the diazabutadiene backbone were not observed. The ^1H NMR spectrum of compound **6** in d_6-DMSO shows a singlet at δ 2.06 ppm, a triplet at δ 7.10 ppm and a doublet at δ 7.20 ppm, which correspond to the methyl groups, the *p*- and the *m*-protons of the phenyl rings, respectively. The $^{13}C\{^1H\}$ NMR (d_6-DMSO) spectrum exhibits the expected peaks for the phenyl rings. For compounds **5** and **6** no signals were observed for the quaternary imine carbon atoms. In both cases, after 24 h in d_6-DMSO solvent, some substitution of the ligand by the solvent was observed in the ^1H NMR spectra, forming [$PdCl_2(DMSO)_2$] and free ligand [PhN=C(Cl)–C(Cl)=NPh] (**1**) or [($2,6\text{-}Me_2C_6H_3$)N=C(Cl)–C(Cl)=N($2,6\text{-}Me_2C_6H_3$)] (**2**). The IR spectra of **5** and **6** exhibit signals for $\nu_{C=N}$ at 1554 cm^{-1} and at 1550 cm^{-1} respectively. The stretching frequencies $\nu_{C=N}$ were shifted to lower wavenumbers with respect to those found for the corresponding free ligands [PhN=C(Cl)–

---

[1] The octahedral Ni(II) compound **4** was tested as a catalyst towards the ethylene polymerisation under mild conditions (as described above) but no significant catalytic activity was observed and further investigations of this system were not carried out.

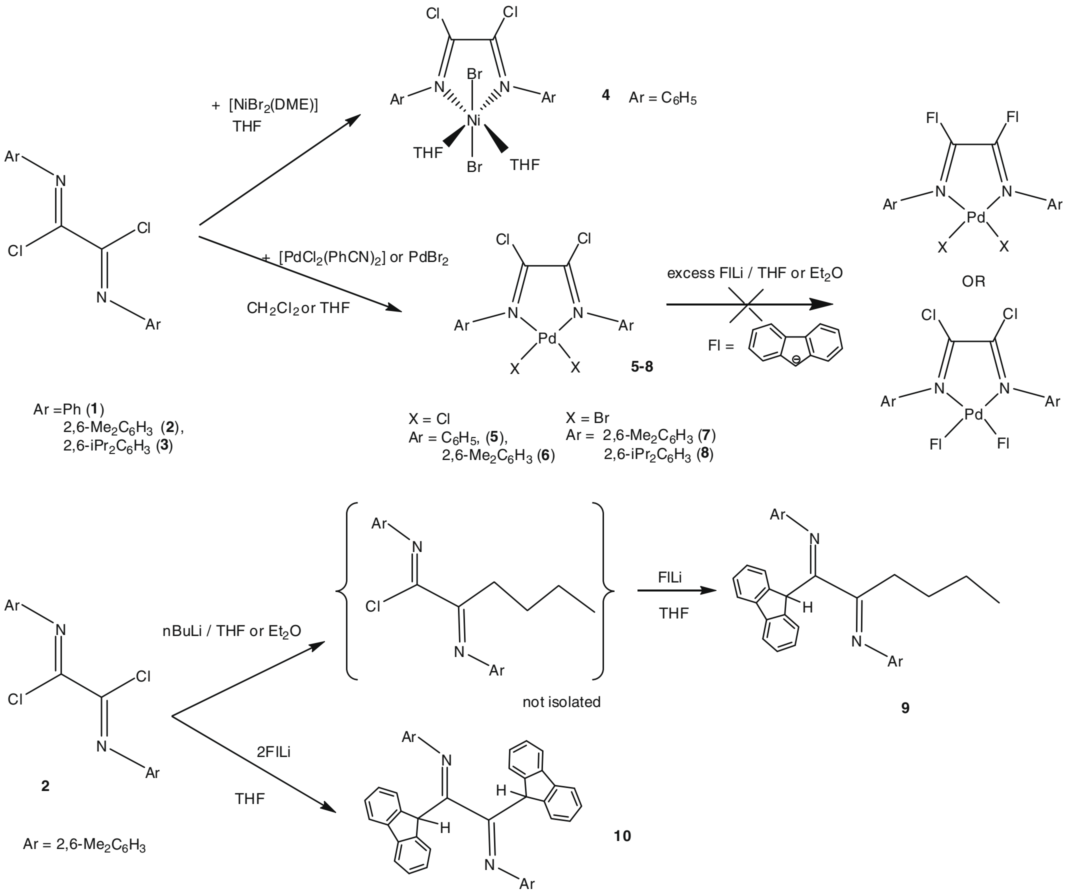

Scheme 1. Reactivity of ligands **1–3** towards Group 10 metal complex precursors and alkylating agents.

C(Cl)═NPh] (**1**) (1664 cm^{-1}) and [(2,6-Me$_2$C$_6$H$_3$)N═C(Cl)–C(Cl)═N(2,6-Me$_2$C$_6$H$_3$)] (**2**) (1660 cm^{-1}), confirming the metal coordination in both cases. Formation of the **7** was confirmed by ^{1}H NMR spectroscopy, mass spectroscopy and elemental analysis. A ^{1}H–^{1}H COSY NMR experiment showed the coupling between the methyl protons at δ 7.00 and the aromatic protons at δ 2.10 and FAB$^+$ spectrum confirmed the presence of the fragment corresponding to [complex – 2Br]$^+$. The ^{1}H NMR spectrum of [PdBr$_2${(2,6-^{i}Pr$_2$C$_6$H$_3$)N═C(Cl)}$_2$)] (**8**) showed a downfield shift of the diimine ligand resonances. For example, the C*H*Me$_2$ resonances were found at δ 2.94 compared with δ 2.80 in the ^{1}H NMR spectra of the free diimine. The ^{1}H–^{1}H COSY experiment shows the coupling of the methyl protons at δ 1.275 and the aromatic protons at δ 7.34 and δ 7.22. Elemental analysis confirmed the formation of the desired product and the FAB$^+$ mass spectrum confirmed the presence of the molecular ion in the correct isotopic pattern. Further evidence is provided by the IR spectrum of **7**, where the $\nu_{C=N}$ was found shifted to a lower wavenumber (1552 cm^{-1} compared with $\nu_{C=N}$ 1664 cm^{-1} in the free ligand **3**, Table 1) Although the choice of solvent and reaction conditions varied with the solubility requirements of each system, mild synthetic routes led to the facile formation of novel complexes of the type [PdX$_2${(2,6-R$_2$C$_6$H$_3$)N═C(Cl)}$_2$] (where R = H, Me, ^{i}Pr, X = Cl or Br). The presence of chlorine atoms at the α-diimine backbone did not seem to hinder the Pd(II) coordination of the ligand.

Table 1
Selected IR data (KBr) corresponding to metal-coordinated (where M = Ni(II) for compound **4** and M = Pd(II) for compounds **5–8**) as well as free oxazolyl chloride ligands (compounds **1–3**).

Ligands		$\nu_{C=N}$ (cm^{-1})	Complexes		$\nu_{C=N}$ (cm^{-1})
			R = Ph	**4**	1590
R = 2,6-Me$_2$C$_6$H$_3$	**1**	1664	R = Ph	**5**	1554
R = 2,6-Me$_2$C$_6$H$_3$	**2**	1660	R = 2,6-Me$_2$C$_6$H$_3$	**6**	1550
R = 2,6-^{i}Pr$_2$C$_6$H$_3$	**3**	1660	R = 2,6-Me$_2$C$_6$H$_3$	**7**	1552
			R = 2,6-^{i}Pr$_2$C$_6$H$_3$	**8**	1552

The reaction of the free ligand [2,6-Me$_2$C$_6$H$_3$)N═C(Cl)}$_2$] (**2**) with one equivalent of ^{n}BuLi (in THF, −78 °C to room temperature), followed by the *in situ* reaction with one equivalent of fluorenyl lithium (from −78 °C to room temperature) led to the clean and complete substitution of the chlorinated ligand backbone. The formation of the new, potentially multidentate, neutral ligand [(2,6-Me$_2$C$_6$H$_3$)N═C(^{n}Bu)–C(Fl)═N(2,6-Me$_2$C$_6$H$_3$)] **9** in ca 15% yield was observed. Similarly, the backbone substitution of the free ligand [2,6-Me$_2$C$_6$H$_3$)N═C(Cl)}$_2$] **2** using two equivalents of fluorenyl lithium (−78 °C to room temperature) led to the conversion to the new neutral, potentially multidentate ligand precursor [(2,6-Me$_2$C$_6$H$_3$)N═C(Fl)–C(Fl)═N(2,6-Me$_2$C$_6$H$_3$)] **10** in ca. 65% yield. The compounds **9** and **10** were characterised by FAB$^+$ mass spectrometry, IR (KBr), ^{1}H NMR, ^{13}C{^{1}H} NMR and X-ray diffraction. We have thus obtained two unusual ligands having the potential to support new heterobimetallic α-diimine/metallocene pre-catalyst systems. These complexes were characterised in the solid state by X-ray crystallography. They could potentially combine the 4-electron donor abilities of α-diimines with up to 6-electron donor (when deprotonated) of a fluorenyl unit. These ligand precursors open up new exciting metal coordination possibilities since they could have the potential to coordinate in a variety of modes to both late and/or early transition metals. Studies are in progress to further develop this chemistry for tandem homogeneous catalysis applications.

2.2. X-ray diffraction studies

The molecular structures of free ligands **1**, **9** and **10** and metal complexes **4**, **5** and **7** were determined by single crystal X-ray diffraction. Selected bond distances and angles are shown in Table 1 and crystallographic details in Table 2. ORTEP diagrams describing these structures are represented in Figs. 2–7. Compounds **1**, **9** and **10** were crystallised from deuterated toluene and their X-ray diffraction structures determined. They all show *s-trans* geometries and bond lengths and angles within the expected range for free diimine ligands (e.g. C=N distances of 1.2520(16) Å for **1**, 1.2749(18) and 1.2776(18) Å for **9** and 1.273(3) Å for **10**; and backbone C–C distances of 1.497(2), 1.5070(18) and 1.526(4) Å for **1**, **9** and **10**, respectively. Single crystals suitable for X-ray diffraction of $[NiBr_2(\{PhN{=}C(Cl)\}_2)(THF)_2]$ **4** were obtained by vapour diffusion of pentane into a THF solution of compound **4** at room temperature. This complex adopts a distorted octahedral coordination geometry with the bromine atoms located *trans* to each other and the THF molecules *cis* to each other. The Ni–Br bond lengths averaging 2.534 Å are similar to those for the octahedral complexes $[NiBr_2(\{(p\text{-Tol})N{=}C(Cl)\}_2)(THF)_2]$ (2.535(3) and 2.517(3) Å) [14] and $[NiBr_2(\{(2\text{-}(C_6F_5)C_6H_4)N{=}C(Cl)\}_2)(OH_2)_2]$ (2.439(1) and 2.612(8) Å) [15]. The Ni–O (2.089(3) and 2.081(3) Å) and Ni–N

Table 2
Selected bond lengths (Å) and angles (°) for the free ligands **1**, **9** and **10** and for complexes **4, 5** and **7**.

Comp.	Distances (Å)		Angles (°)	
1	Cl(1)–C(1)	1.7601(12)	C(1)’–C(1)–Cl(1)	112.61(11)
	N(1)–C(2)	1.4191(14)	C(1)’–C(1)–N(1)	122.00(13)
	N(1)–C(1)	1.2520(16)		
	C(1)–C(1’)	1.497(2)		
4	Ni(1)–Br(1)	2.5470(6)	Br(1)–Ni(1)–Br(2)	173.29(3)
	Ni(1)–N(1)	2.094(4)	O(1)–Ni(1)–O(2)	88.20(15)
	Ni(1)–O(1)	2.089(3)	Br(2)–Ni(1)–O(1)	91.02(9)
	Cl(1)–C(1)	1.734(4)	Br(2)–Ni(1)–O(2)	92.92(9)
	N(1)–C(1)	1.261(6)	Br(1)–Ni(1)–N(2)	87.14(9)
	N(1)–C(3)	1.437(5)	Br(2)–Ni(1)–N(2)	90.28(9)
	C(1)–C(2)	1.516(5)	O(2)–Ni(1)–N(2)	94.32(14)
	Ni(1)–Br(2)	2.5209(6)	Cl(2)–C(2)–C(1)	118.2(3)
	Ni(1)–N(2)	2.104(3)	C(1)–C(2)–N(2)	116.7(3)
	Ni(1)–O(2)	2.081(3)	N(1)–Ni(1)–N(2)	78.31(13)
	Cl(2)–C(2)	1.734(4)	Br(1)–Ni(1)–O(1)	91.28(9)
	N(2)–C(2)	1.268(6)	Br(1)–Ni(1)–O(2)	93.45(9)
	N(2)–C(9)	1.433(5)	Br(1)–Ni(1)–N(1)	87.00(9)
			Br(2)–Ni(1)–N(1)	86.42(9)
			O(1)–Ni(1)–N(1)	99.19(14)
			Cl(1)–C(1)–C(2)	118.5(3)
			C(2)–C(1)–N(1)	116.5(4)
5	Pd(1)–Cl(3)	2.2548(9)	N(1)–Pd(1)–N(2)	80.15(11)
	Pd(1)–N(1)	2.043(3)	Cl(3)–Pd(1)–N(1)	92.80(7)
	Cl(1)–C(1)	1.704(3)	Cl(1)–C(1)–C(2)	119.0(3)
	N(1)–C(1)	1.277(4)	Pd(1)–N(2)–C(2)	112.4(2)
	N(1)–C(3)	1.432(4)	Pd(1)–N(2)–C(9)	127.1(2)
	C(1)–C(2)	1.478(5)	Cl(3)–Pd(1)–Cl(4)	91.15(3)
	Pd(1)–Cl(4)	2.2848(9)	Cl(4)–Pd(1)–N(2)	95.85(8)
	Pd(1)–N(2)	2.060(3)	Cl(2)–C(2)–C(1)	118.8(3)
	Cl(2)–C(2)	1.698(3)	Pd(1)–N(1)–C(1)	113.2(2)
	N(2)–C(2)	1.281(5)	Pd(1)–N(1)–C(3)	125.0(2)
	N(2)–C(9)	1.438(4)		
7	Pd(1)–N(1)	2.045(3)	N1–Pd1–N2	79.43(11)
	Pd(1)–N(2)	2.054(3)	Br1–Pd1–Br2	90.656(19)
	Pd(1)–Br(1)	2.3747(7)	Br1–Pd1–N1	93.88(8)
	Pd(1)–Br(2)	2.3966(4)	Br2–Pd1–N1	174.81(8)
	N(1)–C(1)	1.279(4)	Br1–Pd1–N2	170.31(9)
	N(1)–C(3)	1.449(4)	Br2–Pd1–N2	96.36(8)
	C(1)–Cl(1)	1.697(3)	Pd1–N1–C1	114.1(2)
	C(1)–C(2)	1.503(4)	Pd1–N1–C3	124.6(2)
	N(2)–C(2)	1.277(5)	Pd1–N2–C2	113.8(2)
	N(2)–C(11)	1.444(4)	Pd1–N2–C1)	125.0(2)
	C(2)–Cl(2)	1.695(3)		
9	C(1)–C(2)	1.5070(18)	C(2)–C(1)–C(7)	119.67(12)
	C(1)–C(7)	1.5266(18)	C(2)–C(1)–N(2)	114.98(12)
	C(1)–N(2)	1.2749(18)	C(7)–C(1)–N(2)	125.35(12)
	C(2)–C(3)	1.5141(18)	C(1)–C(2)–C(3)	117.19(12)
	C(2)–N(1)	1.2776(18)	C(1)–C(2)–N(1)	117.12(12)
	C(3)–C(4)	1.524(2)	C(3)–C(2)–N(1)	125.68(12)
			C(2)–C(3)–C(4)	112.71(12)
10	N(1)–C(2)	1.273(3)	C(2)–N(1)–C(29)	123.9(2)
	N(1)–C(29)	1.422(3)	C(3)–N(2)–C(37)	123.3(2)
	N(2)–C(3)	1.272(3)	C(2)–C(1)–C(25)	113.6(2)
	N(2)–C(37)	1.425(3)	C(2)–C(1)–C(28)	116.9(2)
	C(1)–C(2)	1.526(4)		

(2.094(4) and 2.104(3) Å) distances are consistent with those in $[NiBr_2(\{(p\text{-Tol})N{=}C(Cl)\}_2)(THF)_2]$ (2.217(13) and 2.095(12) Å for Ni–O, 2.088(14) and 2.111(14) Å for Ni–N). The C(1)–N(1) and C(2)–N(2) linkages (1.261(6) and 1.268(6) Å, respectively) are of comparable length to those of $[NiBr_2(\{(p\text{-Tol})N{=}C(Cl)\}_2)(THF)_2]$ (averaging 1.252 Å) and longer than those of the related free ligand, $(2,6\text{-}{}^{i}Pr_2C_6H_4)N{=}C(Cl){-}C(Cl){=}N(2,6\text{-}{}^{i}Pr_2C_6H_4)$ (1.245 (av) Å). The C(1)–C(2) bond length of 1.516(5) Å is similar to that for $[NiBr_2(\{(p\text{-Tol})N{=}C(Cl)\}_2)(THF)_2]$ (1.516(25) Å). The C–Cl distances (1.734 (av) Å) are slightly shorter than the corresponding C–Cl distances in $[NiBr_2(\{TolN{=}C(Cl)\}_2)(THF)_2]$ (1.769 (av) Å). The chelate N–Ni–N angle of 78.31(13)° is consistent with the 77.0(5)° found in $[NiBr_2(\{(p\text{-Tol})N{=}C(Cl)\}_2)(THF)_2]$ [14]. The slightly distorted octahedral coordination sphere around the nickel atom can also be seen from the Br(1)–Ni(1)–Br(2) *trans* angle of 173.29(3)°. A similar distorted geometry around the metal centre has been reported earlier for $[NiBr_2(\{(p\text{-Tol})N{=}C(Cl)\}_2)(THF)_2]$ [14]. X-ray quality-single crystals of $[PdCl_2(\{PhN{=}C(Cl)\}_2)]$ **5** were obtained by vapour diffusion of pentane into a CH_2Cl_2 solution of the complex at room temperature. The asymmetric unit cell comprises one molecule of complex **5** showing a slightly distorted square-planar geometry. Distortions from this geometry are indicated by the deviations from a least-squares plane through the following atoms; Pd(1) 0.034, Cl(1) 0.010, Cl(2) −0.026, N(1) −0.031 and N(2) 0.013 Å. A closer examination of the structure reveals an intermolecular interaction between Pd(1)···Cl(2A) of 3.217 Å which seems to be predominantly an electrostatic interaction, between the Pd centre with positive formal charge and the Cl atom with a negative formal charge. The Pd–Cl linkages of 2.270 (av) Å are slightly shorter than those of the related Pd(II) complexes $[PdCl_2(\{(2,6\text{-}{}^{i}Pr_2C_6H_4)N{=}C(H)\}_2)]$ (2.2799(5)–2.2834(5) Å) [27] and $[PdCl_2(Ph{-}BIP)]$ (2.281(4) and 2.282(5)Å) [28]. However, the Pd–N distances of compound **7** (2.052 (av) Å) are slightly longer when compared with the Pd(II)-dihalide complexes mentioned above (2.014(2)–2.025(2) Å), indicating weaker bonding between Pd metal centre and the N atoms of oxalodiimidoyl dichlorides compared with an α-diimine ligand. In **5**, the ligand PhN=C(Cl)–C(Cl)=NPh (**1**) adopts the *s-cis* configuration due to chelation to the metal. The phenyl rings are placed approximately perpendicular to the plane formed by the metal and coordinated nitrogen atoms. In contrast, the related free ligand $(2,6\text{-}{}^{i}Pr_2C_6H_4)N{=}C(Cl){-}C(Cl){=}N(2,6\text{-}{}^{i}Pr_2C_6H_4)$ has *s-trans* geometry to minimise steric interactions [15]. The N=C (1.277(4) and 1.281(5) Å) and C(1)–C(2) bond lengths (1.478(5) Å) are similar to those found in the earlier reported Pd(II) complex above [27] (i.e. 1.269(4) and 1.305(3) for N=C and 1.460(5) and 1.493(4) Å for C—C bond respectively). The longer N=C bond lengths compared with compound **4** (1.261(6) and 1.268(6) Å), suggests a more effective π-back donation from the Pd(II) with respect to Ni(II) probably due to a better overlap of metal and ligand orbitals. The C(1)–C(2) and C–Cl distances of compound **5** are shorter than those of compound **4**, indicating a small degree of electron delocalisation within the N=C(Cl)–C(Cl)=N fragment. X-ray quality single crystals of $[PdBr_2(\{2,6\text{-}Me_2C_6H_3N{=}C(Cl)\}_2)]$ (**7**) were also grown by slow diffusion of pentane into a concentrated solution of the red-orange

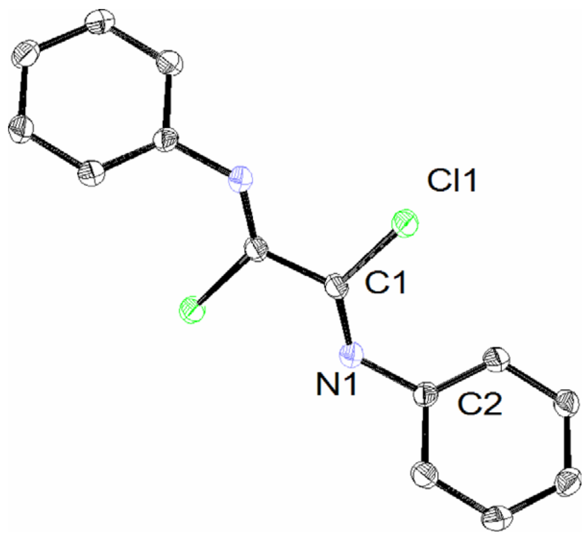

Fig. 2. ORTEP representation of ligand **1** (50% thermal ellipsoids, H atoms are omitted for clarity). Asymmetric unit contains only half molecule, the other half was generated by symmetry.

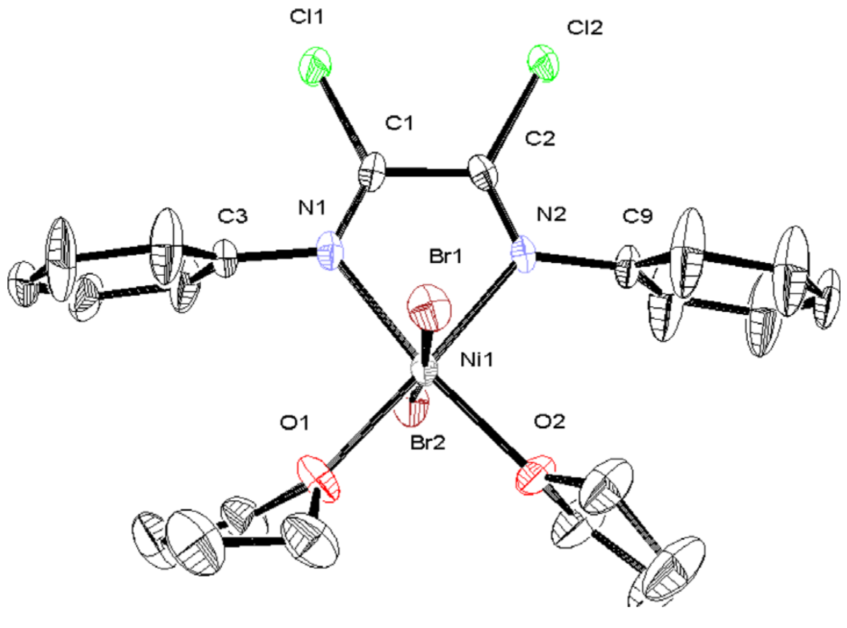

Fig. 3. ORTEP representation of compound **4** (50% thermal ellipsoids, H atoms are omitted for clarity). Each THF molecule was refined as disordered over two positions, with 0.5 occupancy each.

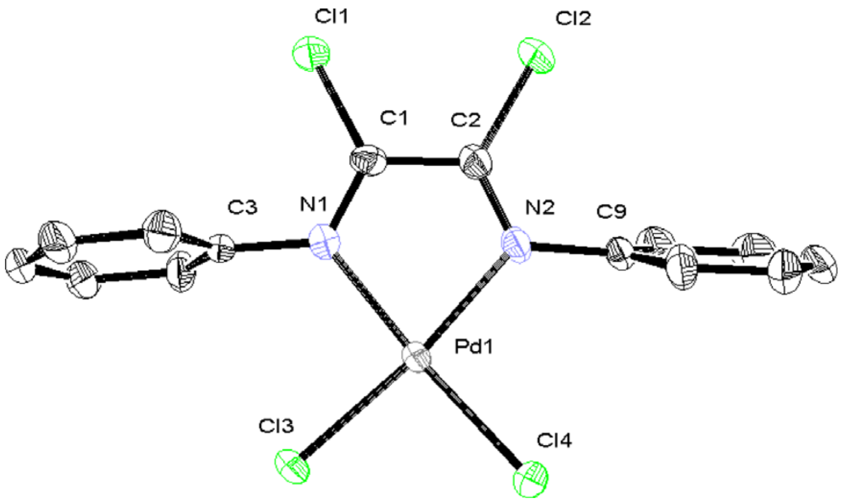

Fig. 4. ORTEP representation of compound **5** (50% thermal ellipsoids, H atoms are omitted for clarity).

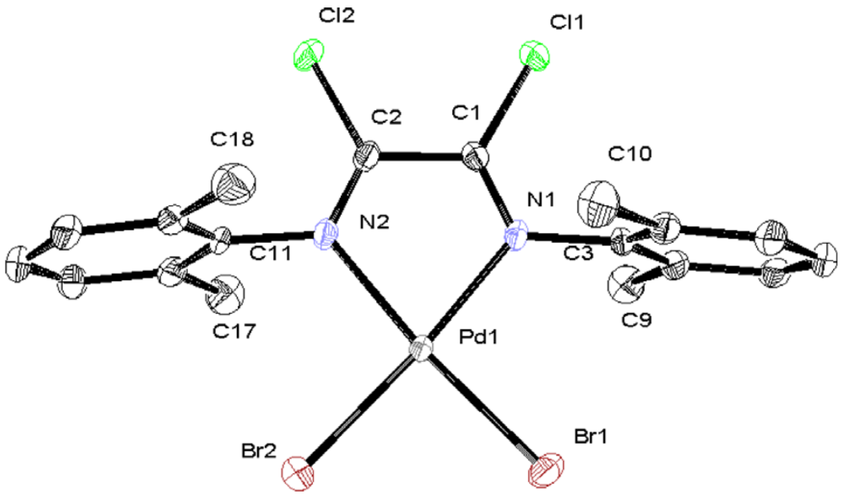

Fig. 5. ORTEP representation of compound **7** (50% thermal ellipsoids, H atoms are omitted for clarity, one of the Br ions was refined as disordered over two positions, with 0.5 occupancy each).

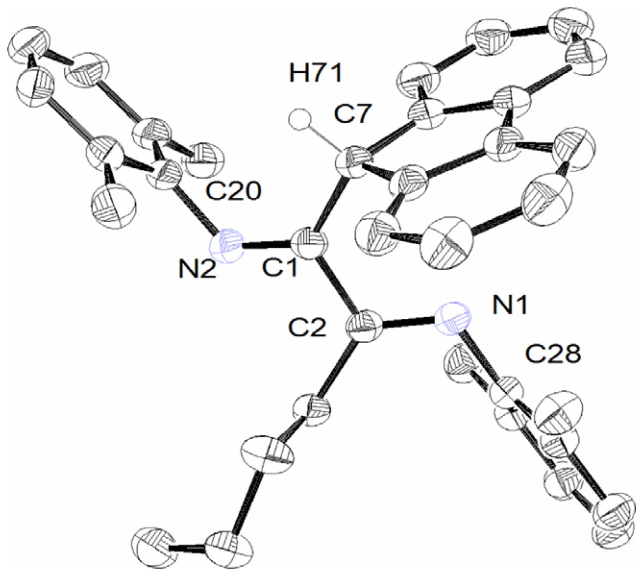

Fig. 6. ORTEP representation of compound **9** (50% thermal ellipsoids).

solid dissolved in CH_2Cl_2. The square planar geometry of the Pd(II) centre in **7** is shown in Fig. 5, with the bromine atoms located slightly above and below the plane of the molecule. All bonds and angles are entirely consistent to those discussed above for the structure of **5**. The bond lengths for the C(1)–C(2) ligand backbone are within the expected range for Pd(II)-coordinated diimines, 1.503(4), and close to those of C–C single bonds (typically 1.54 Å), whilst those for N(1)–C(1) (of 1.279(4) Å) and N(2)–C(2) and (of 1.277(5) Å) indicate metal-coordinated $C{=}N$, as they are longer than those found in free ligand **1** (of 1.2520(16) Å).

2.3. Reactivity of [$PdBr_2\{(2,6\text{-}R_2C_6H_3)N{=}C(Cl)\}_2$] (R = Me, ^{i}Pr) and electronic structures by DFT calculations

To test the reactivity of the Pd(II) complexes formed, and explore possible routes towards isolation of new species based on the further derivatisation of the backbone chlorine ligands, we treated the Pd(II) compounds **7** and **8** with the alkylating reagents lithium fluorenyl, phenyl lithium and CpTMSLi in THF or Et_2O between 0 °C and room temperature (Scheme 1). These tests were carried out in stoichiometric ratios as well as using vast excess of alkylating reagents. Thus far, the substitution reactions between fluorenyl lithium and complex 7 (where ligand **2** is $PdBr_2$-coordi-

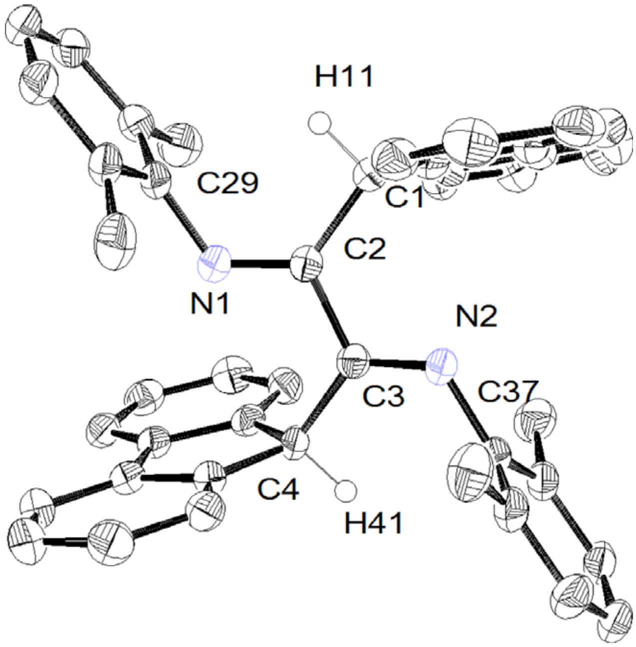

Fig. 7. ORTEP representation of compound **10** (50% thermal ellipsoids).

nated) did not succeed in alkylating the metal centre or in yielding new metal complexes with alkylated ligand backbones (Scheme 1). Instead, only the unreacted starting materials together with small amounts of untractable decomposition products were isolated under the mild conditions applied. The direct conversion into the corresponding alkylated metal complexes could not be demonstrated: it appears that the N-coordinated Pd(II) centre deactivates the chlorine-substituted backbone of these oxazolyl chlorides but further studies are needed to fully understand these reactions.

Group 10 metal complexes of oxazolyl chloride ligands can be regarded structurally as closely related to the Brookhart-type pre-catalysts for olefin polymerisation [2–4]. We are interested in determining whether the replacement of the carbon backbone of typical α-diimine pre-catalysts with chlorine substituents influences their activity and/or the properties of any polymer obtained. Electronic factors, as a result of electron density withdrawal by the chlorine atoms, could affect the activity of the Pd(II) catalysis under the mild conditions. Catalysis tests were thus carried out, under mild conditions, for $[PdBr_2\{2,6\text{-}R_2C_6H_3N{=}C(Cl)\}_2]$ (where R = Me (**7**) and ^{i}Pr (**8**)), using MAO as a co-catalyst (molar ratio Al:Pd ca 310), 2–4 bar ethylene in toluene and 900 minutes reaction time at 25 °C. Pre-catalysts known to act as typical Pd(II) Brookhart-type systems for activation of ethylene (i.e. $[PdBr_2\{(2,6\text{-}Me_2C_6H_3)N{=}C(Me)\}_2]$ (**11**) and $[PdBr_2\{(2,6\text{-}Me_2C_6H_3)N{=}C\}_2Nap]$ (Nap = 1,8-naphthalenyl) (**12**) were also prepared via standard methods [7,29] and tested under the same conditions as described above for **7** and **8**. The behaviour of all Pd(II) pre-catalysts investigated was similar: they all showed very low activities, with only a few mg of PE isolated and activities lower than 0.0002×10^6 g PE/mol × h × bar, and no significant amount of oligomers was identified in the liquid phase by GC–MS for **7**, **8**, **11** and **12**. This behaviour was entirely consistent with that reported earlier for Pd(II) diimines under mild conditions [30]. Although these tests were expected to help us rationalise whether changes in the nature of the backbone substituents affect catalytic properties in the series, the activities of these Pd(II) precursors the olefin polymerisation were all extremely low under the mild conditions employed, regardless of the nature of the backbone and despite the use of significantly longer polymerisation times, higher catalyst loading and higher ethylene pressures than those typically used for Ni(II) diimines [15]. Although the ethylene monomer activation by the Pd(II) centre does seem to take place in all cases, significantly higher temperatures and pressures of monomer may be needed to generate the polymers using these Pd(II) complexes. It would be difficult to assign the precise reasons for the low activity of **7** and **8** by simply comparing the catalytic behaviour towards ethylene polymerisation with those of typical Brookhart-type palladium diimines, as the activity of all Pd diimines tested under these mild conditions was low throughout.

Two initial hypotheses for the low activities of **7** and **8** in the formation of polyethylene may be formulated: (a) electronic factors (essentially as a result of electron density withdrawal by

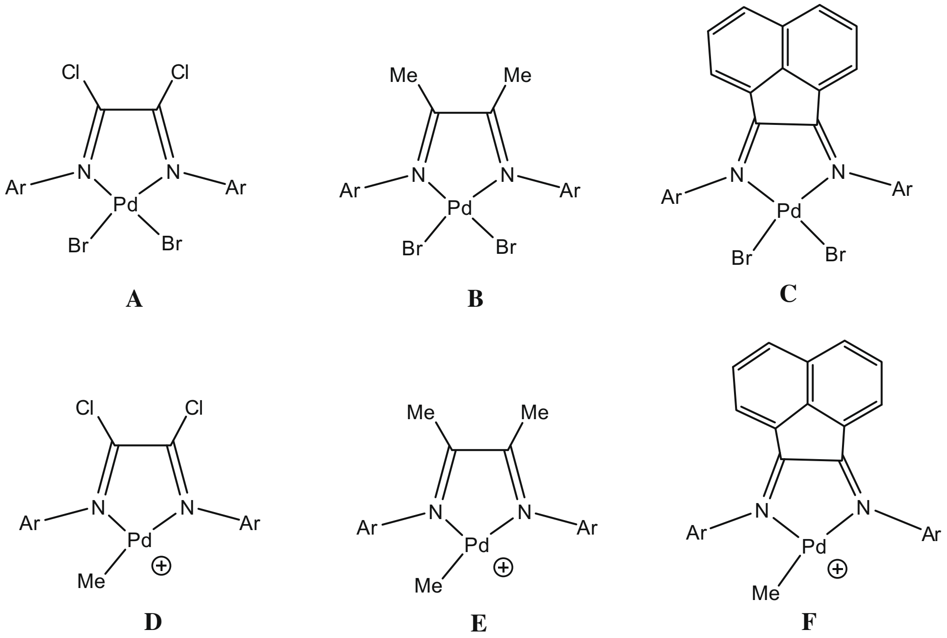

Fig. 8. Representation of DFT-level optimised neutral species **A–C** and cations **D–F**. (Ar = $2,6\text{-}Me_2C_6H_3$).

Table 3
Selected crystallographic data.

	1	**4**	**5**	**7**	**9**	**10**
Empirical formula	$C_{14}H_{10}Cl_2N_2$	$C_{22}H_{26}Br_2Cl_2N_2NiO_2$	$C_{14}H_{10}Cl_4N_2Pd$	$C_{18}H_{18}Br_2Cl_2N_2Pd$	$C_{35}H_{36}N_2$	$C_{44}H_{36}N_2$
Formula weight	277.15	639.89	454.46	599.47	484.68	592.78
Crystal system	monoclinic	monoclinic	orthorhombic	monoclinic	triclinic	triclinic
Space group	*P*21/*n*	*P*21/*n*	*P*212121	*P*21/*a*	$P\bar{1}$	$P\bar{1}$
Unit cell dimensions:						
a (Å)	3.91020(10)	9.6200(1)	7.0602(1)	13.8883(3)	9.7372(3)	10.7683(4)
b (Å)	11.0788(3)	19.0638(2)	22.4867(3)	7.2562(2)	10.3731(3)	12.4459(5)
c (Å)	14.3526(4)	13.6159(2)	9.9806(1)	20.0150(4)	14.5123(5)	12.9726(6)
α (°)	90	90	90	90	109.0433(15)	84.822(2)
β (°)	92.3451(12)	91.5258(5)	90	97.6232(13)	98.6066(17)	75.203(2)
γ (°)	90	90	90	90	93.4458(17)	72.6660(16)
Volume ($Å^3$)	621.24(3)	2496.19(5)	1584.5(1)	1999.2(1)	1360.65(8)	1604.4(1)
Z	2	4	4	4	2	2
Density (calculated) (Mg/m^3)	1.482	1.703	1.905	1.992	1.183	1.227
Absorption coefficient (mm^{-1})	0.503	4.214	1.837	5.197	0.068	0.071
F(0 0 0)	284	1280	886	1154	520	628
θ Range for data collection	5–27	3–27	3–28	5–28	5–25	4–27.5
Index ranges	$-5 < h < 5$ $-14 < k < 14$ $-18 < l < 18$	$0 < h < 12$ $0 < k < 24$ $-17 < l < 17$	$0 < h < 8$ $0 < k < 28$ $-12 < l < 12$	$-18 < h < 18$ $-9 < k < 9$ $-25 < l < 25$	$-12 < h < 11$ $-13 < k < 13$ $-18 < l < 18$	-13 $< h < 14$ $-16 < k < 15$ $-16 < l < 16$
Reflections collected	2613	5893	3426	19 920	10 033	13 421
Independent reflections	1397	5714	3407	4577	6068	7330
Max. and min. transmission	0.9, 0.9	0.78, 0.84	0.86, 0.93	0.39, 0.73	0.99, 0.99	1, 1
Parameters	82	334	191	236	334	415
Goodness-of-fit (GOF)	1.0296	1.0531	0.9956	1.0092	1.0836	1.0474
Final *R* indices	0.0279 $[I > 3\sigma(I)]$	0.0437 $[I>2\sigma(I)]$	0.0250 $[I > 3\sigma(I)]$	0.0327	0.0753	0.0579
Largest diff. peak and hole (e $Å^{-3}$)	−0.26; 0.22	−1.08; 0.82	−0.77; 1.07	−0.98; 0.61	−0.16; 0.17	−0.36; 0.35

Table 4
Experimental and calculated bond lengths (Å) and angles (°) for **7** and model complexes **A**, **B** and **C**.

Comp.	Pd–Br	Pd–N	N–C	C(1)–C(2)	Br–Pd–Br	N–Pd–Br
7 (exp)	2.385 (av)	2.050(av)	1.277(av)	1.503	90.66	95.12
A (calc)	2.387	2.028	1.290	1.450	89.35	95.41
B (calc)	2.400	2.004	1.305	1.451	90.0	95.65
C (calc)	2.390	2.031	1.296	1.462	91.16	94.035

the chlorine atoms resulting in the reduction of electron density on the metal by back donation into the antibonding orbitals of the oxazolyl chloride ligand, which could in turn affect the olefin polymerisation mechanism. (b) MAO is a Lewis acid and it may attack the chlorine atoms on the ligand in preference to (or as well as) the bromine atoms bound to the metal, leading to catalyst decomposition during the initiation stage of the ethylene polymerisation stages. Reactions of **7** with alkylating reagents were not conclusive thus far but seemed to suggest that once coordinated the reactivity of the oxazolyl chloride ligand is significantly reduced.

An insight into the electronic structure of this class of Pd(II) complexes was gained using Density Functional Theoretical calculations (DFT). The gas-phase geometries of $[PdBr_2\{(2,6\text{-}Me_2C_6H_3)N{=}C(Cl)\}_2]$ (compound **7**, gas-phase modelled geometry **A**), $[PdBr_2\{(2,6\text{-}Me_2C_6H_3)N{=}C(Me)\}_2]$ (compound **11**, gas-phase modelled geometry **B**) and $[PdBr_2\{(2,6\text{-}Me_2C_6H_3)N{=}C\}_2Nap]$ (compound **12**, gas-phase modelled geometry **C**, where Nap = 1,8-Naphthalenyl) were optimised without symmetry constrains. Model species **A** and **B** have similar geometries to well established Pd(II) halide precursors in olefin polymerisation catalysis. Their treatment with MAO would be expected to give catalytic species which can be simplified (for the purpose of modelling) as $[PdMe\{(2,6\text{-}Me_2C_6H_3)N{=}C(Cl)\}_2]^+$ (**D**), $[PdMe\{(2,6\text{-}Me_2C_6H_3)N{=}C(Me)\}_2]^+$ (**E**) and $[PdMe\{(2,6\text{-}Me_2C_6H_3)N{=}C\}_2Nap]^+$ (Nap = 1,8-naphthalenyl) (**F**) (Fig. 8).

A comparison of the calculated geometrical parameters for **A** and those obtained from single crystal X-ray diffraction (for **7**) reveals a good agreement between gas-phase models and the solid state structures (Table 3). There is only a slight underestimation of the C–C bond length in the backbone and of the Pd–N bond length. The geometry of the central $C_2N_2PdBr_2$ unit seems only very slightly influenced by the nature of the substituents in the backbone. The calculated Pd–Br bond length in **A** is 2.387 Å, somewhat shorter than in **B** or **C** (2.400 and 2.390 Å, respectively). Also the Pd–N, C–N and C(1)–C(2) distances in **A**, **B** and **C** remain unchanged with the nature of the backbone substituent.

Table 5
Calculated bond lengths (Å) and angles (°) for modelled species **D**, **E** and **F**.

	D	**E**	**F**
Pd–Me	1.994	1.998	1.991
Pd–N(1)	1.999	1.982	1.993
Pd–N(2)	2.121	2.073	2.125
C(1)–N(1)	1.280	1.301	1.285
C(2)–N(2)	1.293	1.292	1.295
C(1)–C(2)	1.464	1.469	1.480
Me–Pd–N(1)	174.19	178.94	178.45
Me–Pd–N(2)	95.69	100.31	97.10
N(1)–Pd–N(2)	79.86	78.90	81.45

The cationic species $[PdMe\{(2,6\text{-}Me_2C_6H_3)N{=}C(Cl)\}_2]^+$ (**D**), $[PdMe\{(2,6\text{-}Me_2C_6H_3)N{=}C(Me)\}_2]^+$ (**E**) and $[PdMe\{(2,6\text{-}Me_2C_6H_3)\text{-}N{=}C\}_2Nap]^+$ (Nap = 1,8-naphthalenyl) (**F**) were also modelled in the gas phase and without any symmetry restrains. All optimised geometries fit well in the observed trends for **A**, **B** and **C**. The changes in molecular parameters are only minor (Tables 4 and 5). The most noticeable difference is a wider Me–Pd–N(2) angle in **E** and **F** than in **D**. This implies a Me–Pd–N(2) angle closer to linearity in **E** and **F**. The C–Cl bond length in the monocationic species **D** (1.694 and 1.704 Å) is only slightly shorter than that calculated for the neutral model complex **A** (1.710 Å).

The analysis of the Hirshfeld charge distribution shows the accumulation of positive charge on palladium (ca. 0.44, 0.44 and 0.43 for **A**, **B** and **C**, respectively) and that of negative charge on bromine and (to much lesser extent) on nitrogen atoms The calculated charges on nitrogens were −0.08 for all complexes, those on bromines were −0.24, −0.27 and −0.26 (for **A**, **B** and **C**, respectively). Unexpectedly the chlorine atoms in compounds **A** and **D** were found slightly positively charged (calculated Hirshfeld value of 0.07). For **D**, **E** and **F**, the varying the backbone substituent from Cl to Me and Nap led to an increase of the positive charge on pal-

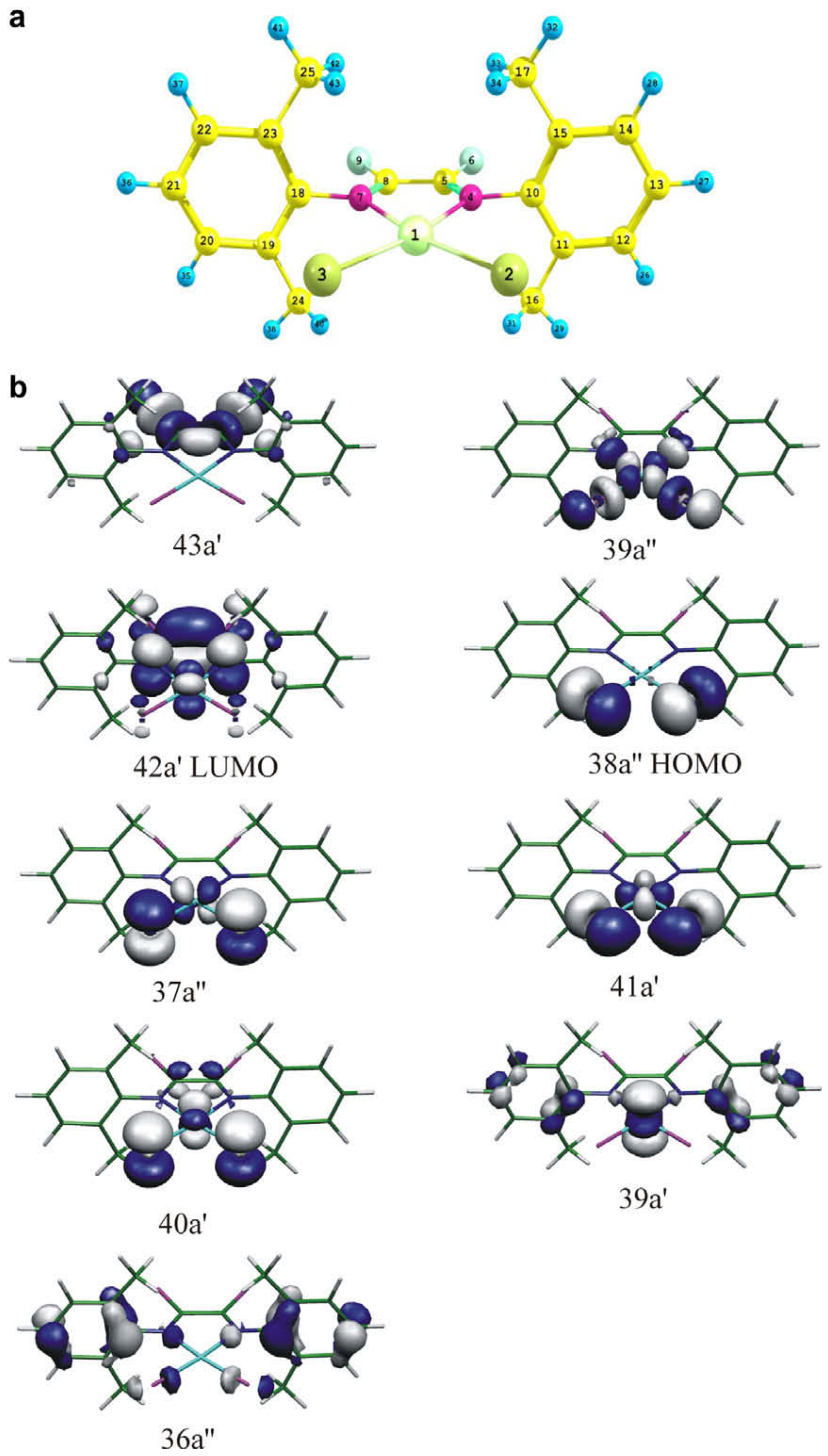

Fig. 9. Optimised geometry of complex **7** (model species **A**, a) and representations of the isosurfaces corresponding to the molecular orbitals of model species **A** (b), **B** (c), **C** (d). Increased label value consistent with increase in orbital energy. Model species **A–C** are isostructural.

ladium centres and a decrease of the negative charge on nitrogens. The magnitude of the charge accumulation on Pd, and charge depletion on N is almost equal for **D**, **E** and **F**. The Hirshfeld, Mulliken and Voronoi charge distributions show similar trends. Our calculations indicate that charge distribution does not seem to be significantly affected by the nature of backbone substituents.

For **A–C** the occupied MOs of highest energy are all centred on the bromine atoms (Fig. 9). The HOMOs of **A** and **B** are mainly formed from the p-orbitals of bromine centres, without significant contribution from palladium. However, HOMO−1 and HOMO−2 show contributions from palladium d orbitals. The shapes and energies of the MO's of C were found qualitatively identical with

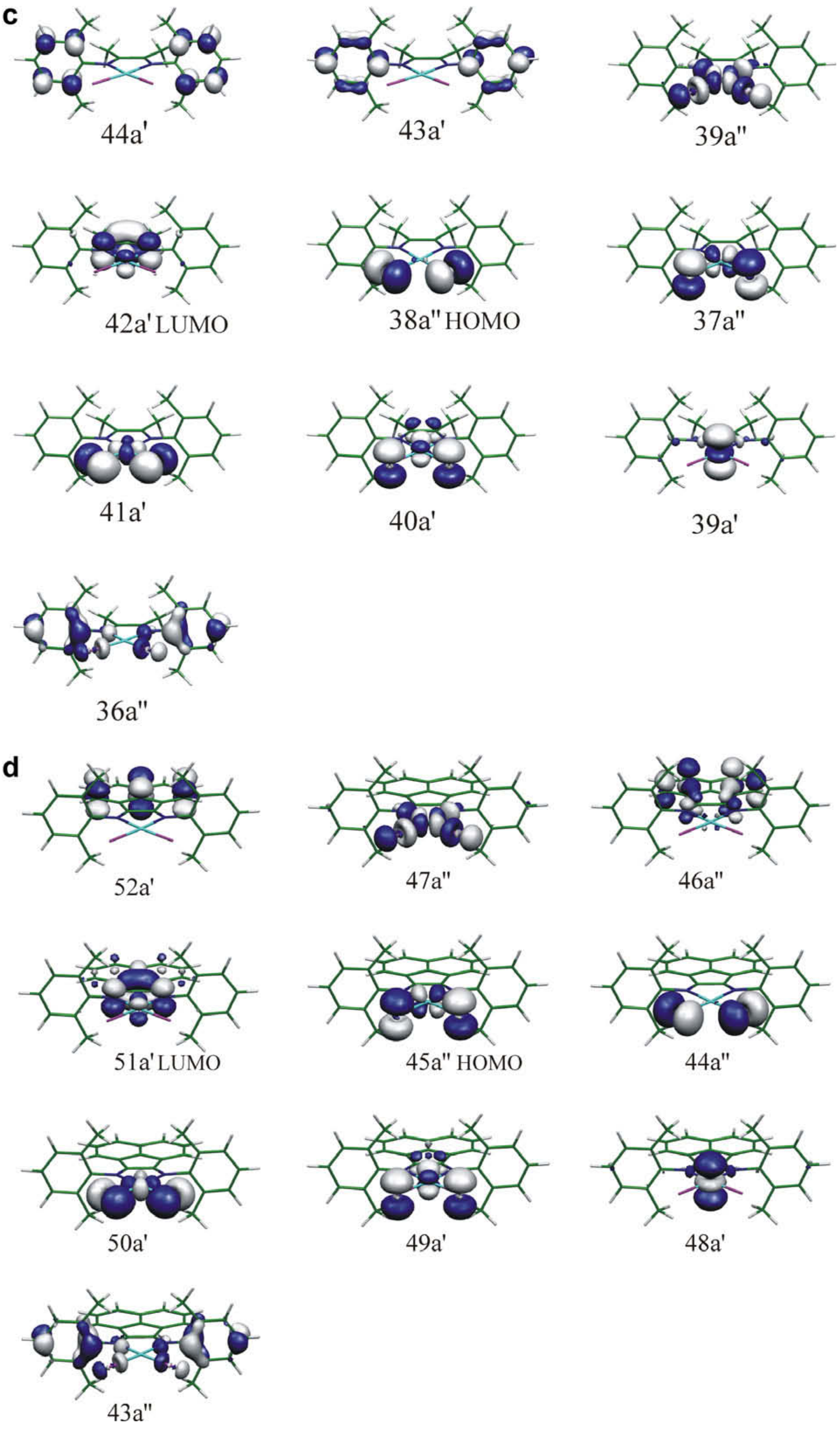

Fig. 9 (*continued*)

those of **A** and **B**. The only difference was that the relative energies of HOMO and HOMO−1 are inverted, although the HOMO/HOMO−1 energy gap is very narrow (0.051 eV). The LUMOs of **A–C** are centred on the delocalised backbone with relatively small contribution from palladium. Complexes **A–C** are all characterised by a relatively high HOMO/LUMO gap.

In [$PdBr_2\{(2,6\text{-}Me_2C_6H_3)N{=}C(Cl)\}_2$] (**A**), the lone pairs of the chlorine substituents at the ligand backbone are much lower in energy than those of the bromine substituents. These calculations suggest that the Lewis acid attack at the C–Cl backbone substituents is unfavourable with respect to that at the Pd–bromine centres. This is consistent with the observation that halogen-containing bis(imino)pyridine metal catalysts were found to be stable to the MAO attack [31]. For **D–F** the HOMOs (shown in Fig. 10) have strong contributions from the methyl group, Pd d-orbitals and from the π system of one aryl ligand. The HOMO−1 and

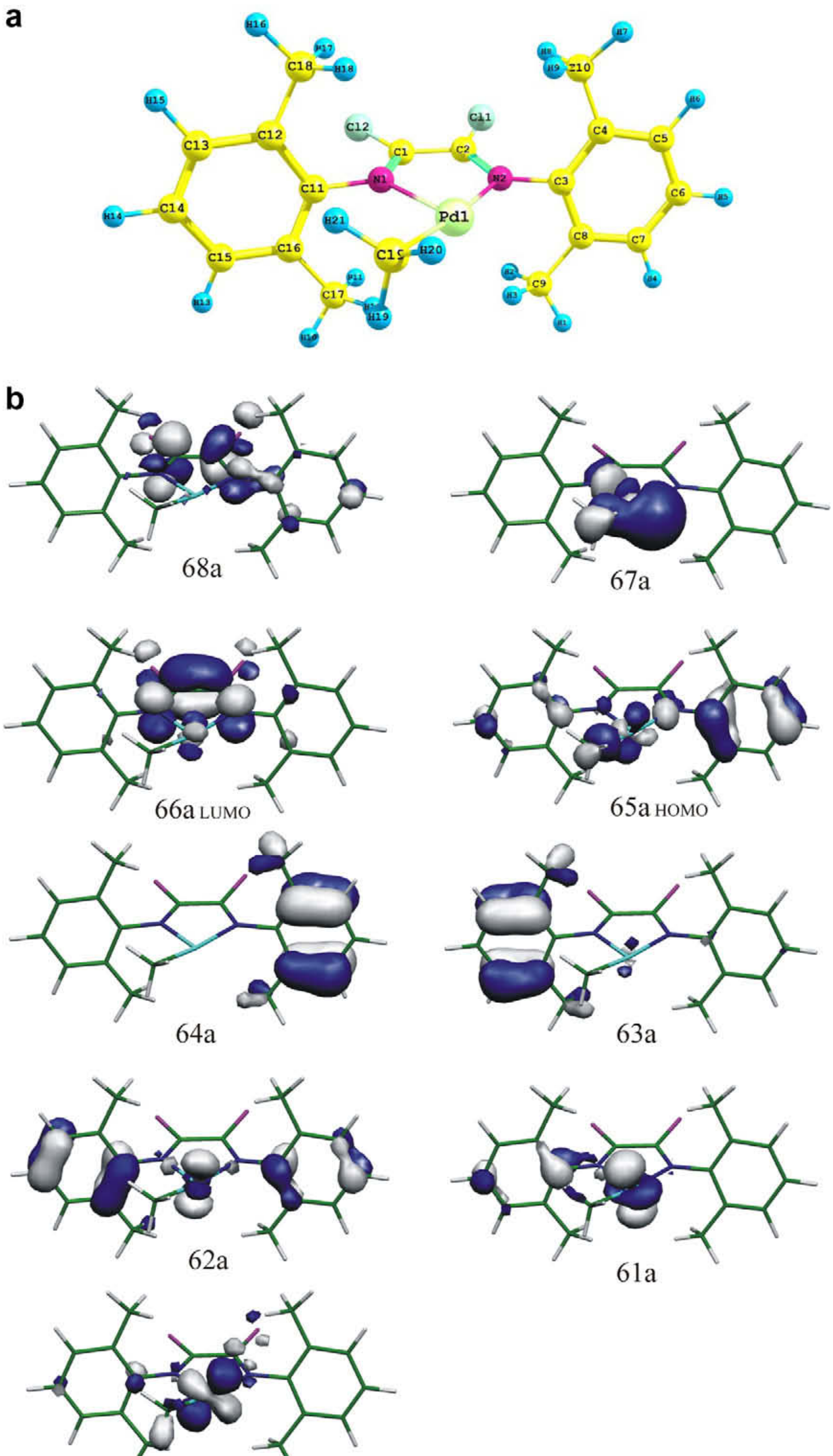

Fig. 10. Optimised geometry of **D** (a) and representations of the isosurfaces corresponding to the molecular orbitals of **D** (b), **E** (c), **F** (d). Increased label value consistent with increase in orbital energy. Model species **D–F** are isostructural.

HOMO−2 in **A** is formed exclusively from π system of the aryl groups, whereas the corresponding orbitals of **E** and **F** show significant contributions from the palladium d-orbitals. The LUMO in **D–F** is qualitatively identical with the LUMO in **A–C**. The LUMO+1

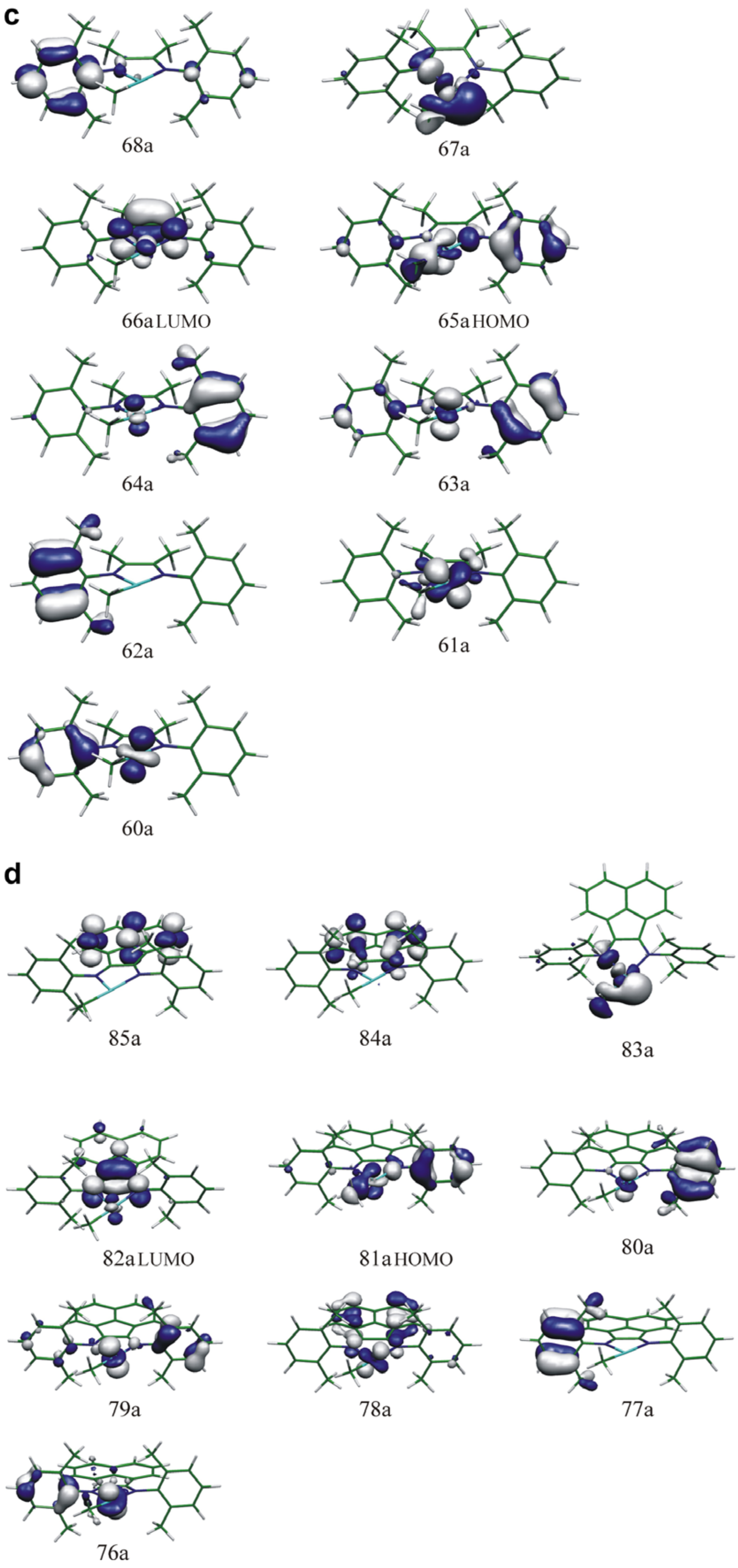

Fig. 10 (*continued*)

orbitals have a relatively high palladium contribution. It is expected that this orbital would play an important role in the binding of the ethylene to cations such as $[PdMe\{(2,6\text{-}Me_2C_6H_3)N{=}C(Cl)\}_2]^+$ (**D**) during the initiation step of the polymerisation reaction. The HOMO/LUMO−1 gaps (158.8, 169.4 and 170.7 kJ/mol for **D**, **E** and **F**, respectively) are within the same range for all three species. The same is true for the HOMO/LUMO gap (of 144.3, 152.5 and 156.3 kJ/mol for **D**, **E** and **F**, respectively). The binding energy of ethylene to **D** (−120.36 kJ/mol) is very close to that of binding to **E** (−121.07 kJ/mol) and **F** (−117.19 kJ/mol).

The inspection of these molecular orbitals suggests that there are no significant thermodynamic differences between the electronic structure of **A** and those of typical Brookhart-type pre-catalyst models **B** and **C**. The catalytic cycle of the ethylene polymerisation with typical α-diimine type catalysts was studied extensively [32–39]. The estimated bonding energies of ethylene to Pd-cations proved that the resulting π-complexes should have similar thermodynamic stabilities regardless of the presence of electron withdrawing substituents at the C–C bridge for **7**. The inactivity of **7** (and, similarly that of **8**) towards the ethylene polymerisation reaction in presence of MAO is likely to be of a kinetic nature: stronger reaction conditions are likely to render this class of complexes as catalytic towards olefin polymerisation, as their electronic configurations, in addition to structural similarities, seem to mimic closely those of typical Brookhart-type α-diimines with well understood catalytic behaviour.

3. Conclusions

New Ni(II) and Pd(II) α-diimines of the type $[MX_2\{ArN{=}C(Cl)\}_2]$ have been prepared and characterised. These complexes are inactive toward ethylene polymerisation catalysis under mild conditions in the presence of MAO. The presence of chlorides as the ligand backbone substituent does not seem to affect the electronic structure in the pre-catalyst series: $[PdBr_2\{(2,6\text{-}Me_2C_6H_3)N{=}C(R\}_2]$, where R = Cl, Me and Nap = 1,8-naphthalenyl as shown by DFT calculations, and the lack of activity in the ethylene oligomerisation reaction needs to be assigned to kinetic factors. The behaviour of Pd(II)–oxazolyl chloride complexes as catalysts in other typical organic coupling reactions (e.g. Heck coupling reactions) needs to be tested to explore their catalytic potential more widely.

4. Experimental details

All manipulations of air- and/or moisture-sensitive materials were carried out under an inert atmosphere of dinitrogen or argon using standard Schlenk line techniques, or in an inert atmosphere dry box containing dinitrogen. Dinitrogen was purified by passage through columns filled with molecular sieves (4 Å) and either manganese (II) oxide suspended on vermiculite for the vacuum line, or BASF catalyst for the dry box. Argon was purchased from BOC and used as received. Filtrations were performed using modified stainless steel cannulae, which had been fitted with glass fibre filter discs. Solvents and solutions were transferred through stainless steel or Teflon cannulae, using a positive pressure of inert gas. All glassware and cannulae were thoroughly dried at 150 °C before use.

MAO (10% w/w in toluene) was purchased from Witco and used as supplied. All solvents used in the preparation of air-sensitive compounds were pre-dried over activated molecular sieves (4 Å) and then distilled under dinitrogen over the appropriate drying agent: toluene, benzene, THF and light petroleum (bp 40–60 °C) were distilled over sodium metal; Et_2O and pentane were distilled over sodium–potassium alloy; CH_2Cl_2 was dried over CaH_2; EtOH and MeOH were dried over magnesium turnings and iodine. Deuterated solvents were degassed using three consecutive freeze–pump–thaw cycles and kept over molecular sieves (4 Å) (d_6-DMSO) or vacuum distilled from potassium (d^8-toluene) or CaH_2 (CD_2Cl_2, $CDCl_3$). Solution NMR spectra were recorded using either a Varian Mercury 300 (^{1}H: 300 MHz, ^{13}C: 75.5 MHz) or a Varian UNITY*plus* (^{1}H: 500 MHz, ^{13}C: 125.7 MHz) spectrometer, and at room temperature unless otherwise stated. The spectra were referenced internally relative to the residual protio-solvent (^{1}H) and solvent (^{13}C) resonances relative to tetramethylsilane (^{1}H, ^{13}C, $\delta = 0$). Chemical shifts (δ) are expressed in ppm and coupling constants (J) in Hz. Elemental analyses were performed by the Microanalytical Department of the Inorganic Chemistry Laboratory, Oxford. Infra-red spectra were recorded on a 6020 Galaxy Series FT-IR or a Perkin–Elmer 1600 Series FT-IR instrument in the range 4000–400 cm^{-1}. Samples were prepared in the glovebox as pellets in KBr, and data are quoted in wavenumbers (cm^{-1}). All mass spectrometry was carried out at the EPSRC Mass spectrometry service, Swansea.

4.1. Computational details

DFT calculations were carried out using the Amsterdam Density Functional program suite ADF 2004.01 or ADF 2005.01 [40–43]. Scalar relativistic corrections were included in all calculations using the ZORA method [44–48]. The generalised gradient approximation was employed, using the local density approximation of Vosko, Wilk and Nusair [49] together with the nonlocal exchange correlation of Becke [50,51] and the nonlocal correlation correction of Perdew [52]. The TZP basis sets were used with triple-ζ accuracy of Slater type orbitals and two polarisation functions added. The core electrons of the atoms were frozen up to 1s for C and N, 2p for Cl, 3p for Br and 4p for Pd. All quoted electronic structure data from optimised structures use an integration grid of 4.0 and have a gradient correction applied after the SCF cycles.

4.2. X-ray diffraction studies

For single crystal X-ray diffraction all data collections were performed using an Enraf-Nonius KappaCCD diffractometer with graphite-monochromated Mo Kα radiation, ($\lambda = 0.71073$ Å). Intensity data were processed using the DENZO-SMN package [53]. For **10**, crystals were extremely small and weakly diffracting and a laboratory source (KappaCCD) as well as synchrotron radiation at SRS Daresbury, Station 9.8 synchrotron source were used for data collection ($\lambda = 0.69390$). Data from the crystal measured on the laboratory source showed better completion and is reported here.

The crystal structures were solved using the direct-methods program SIR92 [54], which located all non-hydrogen atoms. Subsequent full-matrix least-squares refinement was carried out using the CRYSTALS program suite [55]. Coordinates and anisotropic thermal parameters of all non-hydrogen atoms were refined. The H atoms were positioned geometrically after each cycle of refinement. A Chebychev weighting scheme was applied in addition to an empirical absorption correction [56].

4.3. Reagents and starting materials

PCl_5, $(2,6\text{-}Me_2C_6H_3)NH_2$, $(2,6\text{-}{}^iPr_2C_6H_3)NH_2$, acetic acid, *p*-tosylsulphonic acid and $ClC({=}O){-}C({=}O)Cl$ (Aldrich) were used as supplied. $PhNH_2$ (Aldrich) was dried over CaH_2 and distilled before use. $PhN{=}C(Cl)C(Cl){=}NPh$ (**1**), $(2,6\text{-}Me_2C_6H_3)N{=}C(Cl)C(Cl){=}N(2,6\text{-}Me_2C_6H_3)$ (**2**) and $(2,6\text{-}{}^iPr_2C_6H_3)N{=}C(Cl){-}C(Cl){=}N(2,6\text{-}{}^iPr_2C_6H_3)$ (**3**) were prepared following literature methods [13,26]. The known ligands $[2,6\text{-}Me_2C_6H_3)N{=}C(Me)\}_2]$ and $[\{(2,6\text{-}Me_2C_6H_3)N{=}C\}_2Nap]$ were also prepared according to the literature methods [7,29]. $[NiBr_2(DME)]$, $PdBr_2$ and $[PdCl_2(PhCN)_2]$ (Aldrich) were used as supplied.

*4.4. Synthesis of [NiBr$_2${PhN=C(Cl)}$_2$(THF)$_2$] (**4**)*

A suspension of [NiBr$_2$(DME)] (0.111 g, 0.360 mmol) in THF (30 mL) was added to PhN=C(Cl)–C(Cl)=NPh (**1**) (0.100 g, 0.361 mmol) at room temperature. The resulting orange-red reaction mixture was stirred for 18 h, followed by filtration. The volatiles were removed under reduced pressure and the residue washed with pentane (2 × 5 mL). The crude product was recrystallised from THF/pentane at −20 °C. [NiBr$_2$({PhN=C(Cl)}$_2$)(THF)$_2$], **6** was obtained as an orange crystalline solid (Yield: 0.130 g, 56%).

Elemental analysis: Anal. Calc. for $C_{22}H_{26}Br_2Cl_2N_2NiO_2$: C, 41.3; N, 4.38; H, 4.10. Found: C, 42.03; N, 5.00; H, 4.02%. **IR** (KBr): $\nu_{C=N}$ 1590 cm^{-1}.

*4.5. Synthesis of [PdCl$_2${PhN=C(Cl)}$_2$] (**5**)*

A yellow solution of PhN=C(Cl)–C(Cl)=NPh (0.100 g, 0.361 mmol) in CH_2Cl_2 (10 mL) was added dropwise at room temperature to a dark orange solution of [PdCl$_2$(PhCN)$_2$] (0.115 g, 0.300 mmol) in CH_2Cl_2 (10 mL). The reaction mixture was stirred for a further 60 h, after which time an orange precipitate had formed. The volatiles were removed under reduced pressure to afford an orange solid, which was washed with pentane (2 × 10 mL) and recrystallised from CH_2Cl_2/pentane. [PdCl$_2$({PhN=C(Cl)}$_2$)], **9** was obtained as an orange crystalline solid (yield: 0.082 g, 60%). The above procedure, but using [PdCl$_2$(COD)] (0.086 g, 0.300 mmol) in THF (10 mL) only resulted in the recovery of starting materials.

Elemental analysis: Anal. Calc. for $C_{14}H_{10}Cl_4N_2Pd$: C , 37.00; N, 6.16; H, 2.22. Found: C, 37.01; N, 5.83; H, 2.71%.

IR (KBr): $\nu_{C=N}$ 1554 cm^{-1}. **^{1}H NMR** (d_6-DMSO, 500 MHz, 298 K): *m*-NPh 7.54 (t, 2H, $^3J_{HH}$ = 7.3) *p*-NPh 7.35 (t, 1H, $^3J_{HH}$ = 7.3) *o*-NPh 7.15 (t, 2H, $^3J_{HH}$ = 7.3). **^{13}C{^{1}H}NMR** (d_6-DMSO, 125.7 MHz, 298 K) *ipso*-NPh 137.41 (s) *p*-NPh 128.64 (s) *o*-NPh 124.51 (s) *m*-NPh 120.24 (s).

*4.6. Synthesis of [PdCl$_2${(2,6-Me$_2$C$_6$H$_3$)N=C(Cl)}$_2$] (**6**)*

A dark orange solution of [PdCl$_2$(PhCN)$_2$] (0.230 g, 0.600 mmol) in CH_2Cl_2 (10 mL) was treated with a yellow solution of (2,6-Me$_2$C$_6$H$_3$)N=C(Cl)–C(Cl)=N(2,6-Me$_2$C$_6$H$_3$) (0.200 g, 0.600 mmol) in CH_2Cl_2 (10 mL) at room temperature. The reaction was stirred for 60 h, after which time the solvent was removed under reduced pressure. The residue was washed with pentane (2 × 20 mL) and recrystallised from CH_2Cl_2/pentane. [PdCl$_2$({(2,6-Me$_2$C$_6$H$_3$)N=C(Cl)}$_2$)], **10** was isolated as an orange solid. Yield: 0.165 g, 54% based on [PdCl$_2$(PhCN)$_2$].

Elemental analysis: Anal. Calc. for $C_{18}H_{18}Cl_4N_2Pd$: C, 42.34; N, 5.49; H, 3.55. Found: C, 42.37; N, 4.97; H, 3.89%.

IR (KBr) $\nu_{C=N}$ 1550 cm^{-1}; **^{1}H NMR** (d_6-DMSO, 500 MHz, 298 K) *m*-NPh 7.20 (d, 4H, $^3J_{HH}$ = 7.8), *p*-NPh 7.10 (t, 2H, $^3J_{HH}$ = 7.8), Me 2.06 (s, 12H)**;** **^{13}C{^{1}H}NMR** (d_6-DMSO, 125.7 MHz, 298 K) *ipso*-NPh 144.03 (s), *C*–Cl 138.53 (s), *p*-NPh 125.41 (s), *m*-NPh 128.14 (s), *o*-NPh 124.76 (s).

*4.7. Synthesis of [PdBr$_2${(2,6-Me$_2$C$_6$H$_3$)N=C(Cl)}$_2$] (**7**)*

THF (100 mL) was added to [PdBr$_2$] (2.752 g, 10.3 mmol) stirred for 1 h at r.t. and cooled to −78 °C. To this, a cooled solution of ligand **2** (3.445 g, 10.3 mmol) in THF (100 mL, −78 °C)) was added dropwise. Stirring continued for 18 h during which time the reaction returned to room temperature. This was followed by filtration. The filtrate was kept and the volatiles were removed to yield the desired complex as a red-orange solid (yield 1.914 g, 31% yield). Crystals suitable for analysis by X-ray diffraction were grown via the slow diffusion (4 days) of pentane into a CH_2Cl_2 solution of 7.

Elemental analysis: Anal. Calc. $C_{18}H_{18}Br_2Cl_2N_2Pd{\cdot}0.5$ THF: C, 37.80; H, 3.49; N, 4.41. Found: C, 37.86; H, 3.34; N, 4.61%.

IR (KBr): $\nu_{C=N}$ 1554 cm^{-1}; **^{1}H NMR** (CD$_2$Cl$_2$, 500 MHz, 298 K): *m*-NPh 7.00 (t, 2H, $^3J_{HH}$ = 7.3) *p*-NPh 7.30 (t, 1H, $^3J_{HH}$ = 7.3) *Me* 2.10 (s, 3H)**;** **^{13}C{^{1}H}NMR** (CD$_2$Cl$_2$, 125.7 MHz, 298 K) *p*-NPh 127.0 (s) *o*-NPh 124.1 (s) *m*-NPh 120.1 (s), 2,6-*Me*$_2$ 16 (s); **FAB$^+$**: 435.20 (37) [M−2Br]$^+$.

*4.8. Synthesis of [PdBr$_2${(2,6-^{i}Pr$_2$C$_6$H$_3$)N=C(Cl)}$_2$] (**8**)*

A yellow solution of ligand **3** (3.321 g, 7.5 mmol) was reacted with [PdBr$_2$] (1.985 g, 7.5 mmol) in THF to give the desired product via an analogous route to that reported above for **7**. Filtration of the reaction mixture gave an insoluble, dark-red solid (yield 1.869 g) and, upon removal of volatiles from the filtrate fraction, an oily red-orange solid. Washing the latter with pentane (20 mL) followed by Et$_2$O (20 mL) and filtration yielded **8** as a bright orange solid, which was dried under reduced pressure over night (yield 0.167 g, 3.1% yield). From the additional solid fractions isolated from the reaction mixture, only the unreacted ligand **3** was isolated and identified by ^{1}H NMR.

Elemental analysis: Anal. Calc. $C_{26}H_{34}Br_2Cl_2N_2Pd$ THF: C, 45.97; H, 5.40; N, 3.57. Found: C, 45.43; H, 5.58; N, 4.05%.

IR (KBr): $\nu_{C=N}$ 1554 cm^{-1}; **^{1}H NMR** (CD$_2$Cl$_2$, 500 MHz, 298 K): *m*-NPh 7.22 (d, 2H, $^3J_{HH}$ = 7.8) *p*-NPh 7.22 (t, 1H, $^3J_{HH}$ = 6.9), *i*Pr 2.94 (q, 2H, $^2J_{HH}$ = 6.3) and 1.28 (dd, 12H, Me, $^2J_{HH}$ = 7.2); **^{13}C{^{1}H}NMR** (CD$_2$Cl$_2$, 125.7 MHz, 298 K) *p*-NPh 130.0 (s), *o*-NPh 124.1 (s), *m*-NPh 120.2 (s), 30 *C*HMe$_2$(s,), CH*Me*$_2$ 24 (broad); **FAB$^+$**: 708.95 (14) [M]$^+$.

*4.9. Synthesis of **9***

A cold (−78) solution of ^{n}BuLi (0.155 g, 6 mmol) in Et$_2$O (30 mL) was added dropwise to a solution of **2** (2 g, 6 mmol) in 50 mL Et$_2$O (−78 °C). The reaction mixture was allowed to reach room temperature with stirring giving a yellow suspension over 15 h. This was cooled again to −78 °C and a cold (−78 °C) solution of fluorenyl lithium in Et$_2$O (1.033 g, 6 mmol) was added dropwise. The mixture was allowed to reach room temperature under stirring, over night. Removals of volatiles afforded a white-yellow solid. From this, compound **9** was extracted in 30 mL toluene. Removal of solvent under reduced pressure yielded 0.436 g of compound **9** as a yellow solid (15% yield).

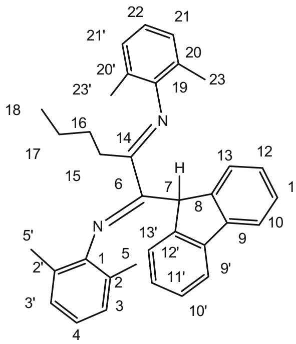

IR (KBr): $\nu_{C=N}$ broad: 1642–1620 cm^{-1}; ^{1}H NMR (C$_6$D$_6$, 500 MHz, 298 K): H10–H13; H10′–H13′: 7.5–7.4 (b multiplet, 8H); H7 4.7 (b, 1H), H3, H3′ 7.01 (d, 2H), H4 6.90 (dd, 1H), H21, H21′ 6.741 (bd, 2H), H22 6.49 (dd, 1H); H15 1.22 (b, 2H), H16 1.15 (b, 2H) H17 0.84 (b, 2H), H18 0.65 (b, 3H); H5, H5′ 2.02 (b, 6H), H23, H23′1.62 (b, 6H); **^{13}C{^{1}H}NMR** (CD$_2$Cl$_2$, 125.7 MHz, 223 K) C14 170.4 (s), C1 and C19 148.2 and 148.5 (overlapped s), C2, C2′, C20, C20′ 125.2 (b), C3, C3′, C20, C20′ 128.2 (b), C4 and C22 123.3 and

123.4 (overlapped s), C7 37.2 (s), C15 30.1 (s), C23, C23′ C5, C5′ 16.2 (b), C18 1.5 (s), C16, C17 2.0 (b), C13, C13′ 127.2 (b), C12, C12′ 129.2 (b), C11, C11′ 124.2 (b), C10, C10′ 123.2 (b); **FAB$^+$**: 485.5 (13) [M]$^+$.

*4.10. Synthesis of **10***

A cold (−78 °C) solution of fluorenyl lithium (2.06 g, 12 mmol) in Et_2O (30 mL) was added dropwise to a solution of **2** (2 g, 6 mmol) in 50 mL Et_2O (−78 °C). The reaction mixture was allowed to reach room temperature under vigorous stirring, giving a yellow suspension over 15 h. Removals of volatiles afforded a yellow solid. From this, compound **10** was extracted in 30 mL toluene. Removal of solvent under reduced pressure yielded compound **10** as a yellow solid (2.31 g, 65% yield).

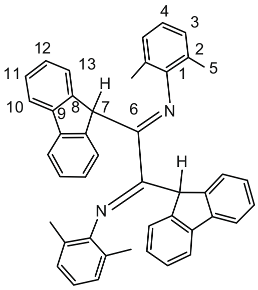

Elemental analysis: Anal. Calc. $C_{44}H_{36}N_2$: C, 89.15; H, 6.12; N, 4.72. Found: C, 85.67; H, 5.79; N, 4.77%.

IR (KBr): $\nu_{C=N}$ 1642 cm^{-1}; ^{1}H NMR (CD_2Cl_2, 500 MHz, 223 K): H3 7.05 (d, 2H, $^3J_{H3-H4} = 7.05$) H4 6.91 (b, 1H), H5 2.01 (s, 6H), H7 3.90 (m, 1H, $^5J_{H7-H12}$ 1.2) H10 7.80 (m, 2H, $^5J_{H10-H13}$ 0.7, $^3J_{H10-H11} = 7.5$) H11 7.37 (m, 2H, $^4J_{H11-H13} = 1.2$ $^3J_{H11-H12} = 7.4$, $^3J_{H10-H11}$ 7.5) H12 7.30 (m, 2H, $^3J_{H12-H13} = 7.4$, $^4J_{H10-H12} = 1.2$, $^3J_{H11-H12} = 7.4$, $^5J_{H7-H12} = 1.2$) and H13 7.56 (m, $^3J_{H12-H13} = 7.4$, $^4J_{H11-H13} = 1.2$, $^5J_{H10-H13} = 0.7$); **^{13}C{^{1}H}NMR** (CD_2Cl_2, 125.7 MHz, 223 K) C1 148.7, C2 125.1, C3 128.2, C4 123.2, C5 18.3, C7 37.2, C8 143.7, C9 141.9, C10 120.1, C11 127.05, C12 127.0, C13 125.4; **FAB$^+$**: 591.37 (8) [M]$^+$.

*4.11. General method for the preparation of Brookhart-type diimines **11** and **12***

An adaptation of reported methods was used [7,29]. Th ligand ([2,6-$Me_2C_6H_3$)N=C(Me)}$_2$] for **11**, or [{(2,6-$Me_2C_6H_3$)N=C}$_2$Nap] for **12**) (1.70 mmol) was dissolved in 10 mL of THF in a Schlenk tube under N_2 atmosphere. In each case, this solution was added via a cannula to a suspension of $PdBr_2$ (0.431 g, 1.62 mmol) in THF (20 mL) and the resulting red-brown mixture was stirred for 3 days, followed by separation by filtration. The filtrate was collected, and the volatiles removed under reduced pressure resulting in orange solids **11** or **12**. The products were washed with 3 × 10 mL pentane, dried under reduced pressure and characterised by elemental analysis, FAB$^+$ mass spectrometry and ^{1}H NMR.

Yields: 0.52 g of **11** (57.5%) and 0.60 g of **12** (56.6%).

*4.11.1. Characterising data **11***

Anal. Calc. for $C_{25}H_{24}Br_2N_2Pd$ THF: C, 45.77; H, 4.96; N, 4.45. Found: C, 45.90; H, 4.55; N, 4.80%; **^{1}H NMR** ($CDCl_3$, 300 MHz, 298 K): *m*-NPh 7.24 (d, 2H, $^3J_{HH} = 7.8$) *p*-NPh 7.22 (t, 1H, $^3J_{HH} = 6.9$), C(*Me*), 2,6-*Me*$_2$ 2.33 (s, 6H), 1.50 (s, 3H); **FAB$^+$**: 482.022(35) [M−Br]$^+$.

*4.11.2. Characterising data **12***

Anal. Calc. for $C_{25}H_{24}Br_2N_2Pd$ THF: C, 52.95; H, 4.30; N, 3.86. Found: C, 52.43; H, 4.24; N, 3.44%; **^{1}H NMR** ($CDCl_3$, 300 MHz, 298 K): Nap ring H^1 8.08 (d, 1H, $^2J_{HH} = 9$), H^2 7.46 (dd, 1H, $^2J_{HH} = 6$), H^3 6.57 (d, 1H, $^2J_{HH} = 9$), *m*-NPh 7.24 (d, 2H, $^3J_{HH} = 7.8$) *p*-NPh 7.22 (t, 1H, $^3J_{HH} = 6.9$), 2,6-Me$_2$ 2.40 (s, 6H); **FAB$^+$**: 575.038(40) [M−Br]$^+$.

4.12. Ethylene polymerisation

MAO (8.5 × 10^{-3} mol Al, in 500 mL toluene) was transferred under Ar to a dried 1-L stainless steel reactor equipped with a magnetic stirrer under 2 bar ethylene pressure at 25 °C. The solution was allowed to stir for 5 min (300 rpm) after which time a solution of the Pd pre-catalyst (27.5 × 10^{-6} mol in 50 mL toluene) was added to the reactor (Al:Pd molar ratio was 310:1). After stirring for 5 min, the reactor contents were degassed and the ethylene pressure controlled between 2 and 4 bar. The reaction mixture was stirred vigorously for 900 min, after which the pressure was released and the reaction quenched with an excess of HCl in MeOH (∼2 M HCl). For each of the pre-catalysts tested (for **7**, **8**, **11** and **12**) only formation of a small amount of PE was observed (less than 300 mg), which was filtered, washed with diluted HCl (to remove Al), water and acetone and dried under reduced pressure. These tests gave extremely low activities (lower than 0.0002 × 10^6 g/mol Pd × h × bar). GC–MS chromatographs and spectra were recorded using a Hewlett Packard 5890 Gas Chromatograph fitted with a non-polar column connected to a Trio-1000 Mass Spectrometer operating Electron Impact (70 eV) and Chemical Ionisation (CI) modes (NH_3). This detected only traces of PE oligomers, as positively charged species.

Acknowledgements

SIP thanks the EPSRC Mass Spectrometry Service, Swansea, Royal Society, St. Anne's College Oxford and University of Bath for funding, STFC for a research grant to support crystallographic work, Drs. Matthew Jones, Stuart Dubberley and Prof. Pedro Gomes for helpful discussions, Dr. Nick Rees for assistance with NMR experiments. GB thanks the Humboldt Foundation and Oxford Supercomputing Centre for funding.

Appendix A. Supplementary material

Supplementary data associated with this article can be found, in the online version, at doi:10.1016/j.ica.2009.11.009.

References

[1] L.K. Johnson, C.M. Killian, M. Brookhart, J. Am. Chem. Soc. 117 (1995) 6414.
[2] M. Brookhart, D.M. Lincoln, J. Am. Chem. Soc. 110 (1988) 8719.
[3] M. Brookhart, A.F. Volpe, D.M. Lincoln, I.T. Hovarth, J.M. Millar, J. Am. Chem. Soc. 112 (1990) 5634.
[4] M. Brookhart, F.C. Rix, D.M. DeSimone, J.C. Barborak, J. Am. Chem. Soc. 114 (1992) 5894.
[5] C.M. Killian, D.J. Tempel, L.K. Johnson, M. Brookhart, J. Am. Chem. Soc. 118 (1996) 11664.
[6] G. VanKoten, K. Vrieze, Adv. Organomet. Chem. 21 (1982) 151.
[7] M. Gasperini, F. Ragaini, S. Cenini, Organometallics 21 (2002) 2950.
[8] R. Bauer, Ber. Deutsch. Chem. Ges. 40 (1907) 2650.
[9] P. Langer, J. Wuckelt, M. Doring, H. Gorls, J. Org. Chem. 65 (12) (2000) 3603.
[10] P.B. Mackenzie, L.S. Moody, C.M. Killian, J.A. Ponasik Jr., J.P. McDevitt, PCT Int. Appl. WO 9840374 A2 19980917, 1998.
[11] J. Wuckelt, M. Doring, P. Langer, H. Gorls, R. Beckert, Tetrahedron Lett. 39 (1998) 1135.
[12] J. Wuckelt, M. Doring, H. Gorls, P. Langer, Eur. J. Inorg. Chem. 3 (2001) 805.
[13] D. Lindauer, R. Beckert, M. Doring, T. Fehling, H. Gorls, J. Prakt. Chem. 337 (1995) 143.
[14] J. Wuckelt, M. Doring, E. Langer, R. Beckert, H. Gorls, J. Org. Chem. 64 (1999) 365.
[15] D.P. Gates, S.A. Svejda, E. Onate, C.M. Killian, D.K. Johnson, P.S. White, M. Brookhart, Macromolecules 33 (2000) 2320.
[16] T. Dohler, H. Gorls, D. Walther, Chem. Commun. (2000) 945.
[17] A.G.J. Ligtenbarg, E.K. van den Beuken, A. Meetsma, N. Veldman, W.J.J. Smeets, A.L. Spek, B.L. Feringa, J. Chem. Soc., Dalton Trans. (1998) 263.

[18] M.E. Broussard, B. Juma, S.G. Train, W.-J. Peng, S.A. Laneman, G.G. Stanley, Science 260 (1993) 1784.
[19] C. Takayama, Y. Yamaguchi, T. Mise, N. Suzuki, J. Chem. Soc., Dalton Trans. (2001) 948.
[20] N. Wheatley, P. Kalck, Chem. Rev. 99 (1999) 3379.
[21] D. Walther, T. Dohler, N. Theyssen, H. Gorls, Eur. J. Inorg. Chem. (2001) 2049.
[22] D. Walther, S. Liesicke, R. Fischer, H. Gorls, J. Weston, A. Batista, Eur. J. Inorg. Chem. (2003) 4321.
[23] S.D. Ittel, L.K. Johnson, M. Brookhart, Chem. Rev. 100 (2000) 1169.
[24] C. Bianchini, A. Meli, Coord. Chem. Rev. 225 (2002) 35.
[25] C.D. Tagge, R.B. Wilson, USA patent, WO 0125 298 A1 2001 0412, 2001.
[26] T.V. Artmonova, A.B. Zhivich, M.Y. Dubinskii, G.I. Koldobskii, Synthesis 12 (1996) 1428.
[27] N.M. Comerlato, G.L. Crossetti, R.A. Howie, P.C.D. Tibultino, J.L. Wardell, Acta Crystallogr. E 57 (2001) m295.
[28] R. van Belzen, R.A. Klein, W.J.J. Smeets, A.L. Spek, R. Benedix, C.J. Elsevier, Recl. Trav. Chim. Pays-Bas 115 (1996) 275.
[29] R. van Asselt, C.J. Elsevier, C. Amatore, A. Jutand, Organometallics 16 (1997) 317.
[30] C. Popeney, Z. Guan, Organometallics 24 (2005) 1145.
[31] Y. Nakayama, K. Sogo, H. Yasuda, T. Shiono, J. Polym. Sci., A: Polym. Chem. 43 (2005) 3368.
[32] L. Deng, P. Margl, T. Ziegler, J. Am. Chem. Soc. 119 (1997) 1094.
[33] L. Deng, T.K. Woo, L. Cavallo, P.M. Margl, T. Ziegler, J. Am. Chem. Soc. 119 (1997) 6177.
[34] R.D.J. Froese, D.G. Musaev, K. Morokuma, J. Am. Chem. Soc. 120 (1998) 1581.
[35] A. Michalak, T. Ziegler, Organometallics 18 (1999) 3998.
[36] D.G. Musaev, M. Svensson, K. Morokuma, S. Stroemberg, K. Zetterberg, P.E.M. Siegbahn, Organometallics 16 (1997) 1933.
[37] T.K. Woo, T. Ziegler, J. Organomet. Chem. 591 (1999) 204.
[38] W. Liu, M. Brookhart, Organometallics 23 (2004) 6099.
[39] D.J. Tempel, L.K. Johnson, R.L. Huff, P.S. White, M. Brookhart, J. Am. Chem. Soc. 122 (2000) 6686.
[40] V.U. Theoretical Chemistry, in: ADF2004.01 SCM, Amsterdam, 2004 <http://www.scm.com>.
[41] V.U. Theoretical Chemistry, in: ADF2005.01 SCM, Amsterdam, 2005 <http://www.scm.com>.
[42] C. Fonseca Guerra, J.G. Snijder, G. Te Velde, E.J. Baerends, Theor. Chem. Acc. 99 (1998) 391.
[43] G. Te Velde, F.M. Bickelhaupt, E.J. Baerends, C. Fonseca Guerra, S.J.A. Van Gisbergen, J.G. Snijders, T. Ziegler, J. Comput. Chem. 22 (2001) 931.
[44] E. Vanlenthe, E.J. Baerends, J.G. Snijders, J. Chem. Phys. 99 (1993) 4597.
[45] E. Vanlenthe, E.J. Baerends, J.G. Snijders, J. Chem. Phys. 101 (1994) 9783.
[46] E. Vanlenthe, E.J. Baerends, J.G. Snijders, J. Chem. Phys. 105 (1996) 6505.
[47] E. Vanlenthe, A. Ehlers, E.J. Baerends, J. Chem. Phys. 110 (1999) 8943.
[48] E. Vanlenthe, R. Van Leeuwen, E.J. Baerends, J.G. Snijders, Int. J. Quantum Chem. 57 (1996) 281.
[49] S.H. Vosko, L. Wilk, M. Nusair, Can. J. Phys. 58 (1980) 1200.
[50] A.D. Becke, Phys. Rev. A 38 (1988) 3098.
[51] A.D. Becke, J. Chem. Phys. 88 (1988) 1053.
[52] J.P. Perdew, Phys. Rev. B 33 (1986) 8800.
[53] Z. Otwinowski, W. Minor, Methods Enzymol. (1997) 276.
[54] A. Altomare, G. Cascarano, G. Giacovazzo, A. Guagliardi, M.C. Burla, G. Polidori, M. Camalli, J. Appl. Crystallogr. 27 (1994) 435.
[55] D.J. Watkin, C.K. Prout, G. Carruthers, P.W. Betteridge, R.I. Cooper, in: Crystals, Oxford, 2001.
[56] N. Walker, D. Stuart, Acta Crystallogr. A 39 (1983) 158.